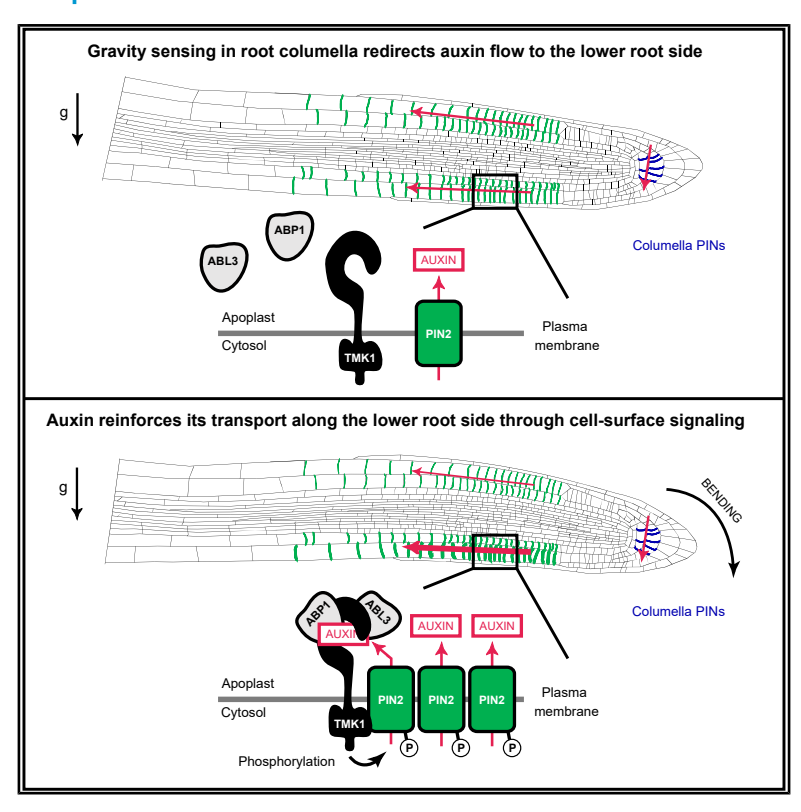


ABP1/ABL3-TMK1 cell-surface auxin signaling targets PIN2-mediated auxin fluxes for root gravitropism

Graphical abstract



Authors

Lesia Rodriguez, Lukáš Fiedler, Minxia Zou, ..., Ivan Kulich, Yvon Jaillais, Jiří Friml

Correspondence

jiri.friml@ista.ac.at

In brief

In gravistimulated roots, gravity perception in the columella redirects the flow of the plant hormone auxin toward the lower root side, where it inhibits cell elongation for downward root bending. This local auxin accumulation activates the cell-surface ABP1/ABL3-TMK1 auxin perception module, which phosphorylates and thus stabilizes the PIN2 auxin exporter for further auxin efflux in a positive feedback loop.

Highlights

- Auxin-inducible, ABP1/TMK1-dependent PIN2 phosphosites function in root gravitropism
- ABP1 acts redundantly with the root-expressed ABL3 receptor
- Auxin induces TMK1 interaction with and phosphorylation of PIN2
- Asymmetric TMK1 activation by auxin mediates asymmetric PIN2 stabilization









Article

ABP1/ABL3-TMK1 cell-surface auxin signaling targets PIN2-mediated auxin fluxes for root gravitropism

Lesia Rodriguez,^{1,6} Lukáš Fiedler,^{1,6} Minxia Zou,¹ Caterina Giannini,¹ Aline Monzer,¹ Dmitrii Vladimirtsev,¹ Marek Randuch,¹ Yongfan Yu,¹ Zuzana Gelová,¹ Inge Verstraeten,¹ Jakub Hajný,^{1,2} Meng Chen,³ Shutang Tan,^{1,3} Lukas Hoermayer,¹ Lanxin Li,¹ Maria Mar Marques-Bueno,^{4,5} Zainab Quddoos,¹ Gergely Molnár,¹ Ivan Kulich,¹ Yvon Jaillais,⁴ and Jiří Friml^{1,7,*}

¹Institute of Science and Technology Austria (ISTA), Am Campus 1, 3400 Klosterneuburg, Austria

²Laboratory of Growth Regulators, The Czech Academy of Sciences, Institute of Experimental Botany & Palacký University, Šlechtitelů 27, 77900 Olomouc, Czech Republic

³MOE Key Laboratory for Cellular Dynamics, Center for Advanced Interdisciplinary Science and Biomedicine of IHM, Hefei National Laboratory for Physical Sciences at the Microscale, Division of Life Sciences and Medicine, University of Science and Technology of China, Hefei 230027, China

⁴Laboratoire Reproduction et Développement des Plantes Université de Lyon, ENS de Lyon, UCB Lyon 1, CNRS, INRAe, 69342 Lyon, France

⁵Present address: Center for Research in Agricultural Genomics (CRAG) CSIC-IRTA-UAB-UB, Barcelona 01893, Spain

*Correspondence: jiri.friml@ista.ac.at https://doi.org/10.1016/j.cell.2025.08.026

SUMMARY

Phytohormone auxin and its directional transport mediate much of the remarkably plastic development of higher plants. Positive feedback between auxin signaling and transport is a prerequisite for (1) self-organizing processes, including vascular tissue formation, and (2) directional growth responses such as gravitropism. Here, we identify a mechanism by which auxin signaling directly targets PIN auxin transporters. Via the cell-surface AUXIN-BINDING PROTEIN1 (ABP1)-TRANSMEMBRANE KINASE 1 (TMK1) receptor module, auxin rapidly induces phosphorylation and thus stabilization of PIN2. Following gravistimulation, initial auxin asymmetry activates autophosphorylation of the TMK1 kinase. This induces TMK1 interaction with and phosphorylation of PIN2, stabilizing PIN2 at the lower root side, thus reinforcing asymmetric auxin flow for root bending. Upstream of TMK1 in this regulation, ABP1 acts redundantly with the root-expressed ABP1-LIKE 3 (ABL3) auxin receptor. Such positive feedback between cell-surface auxin signaling and PIN-mediated polar auxin transport is fundamental for robust root gravitropism and presumably for other self-organizing developmental phenomena.

INTRODUCTION

Plant development differs fundamentally from animals. With cells encapsulated in rigid cell walls without the possibility of migration, plants mainly rely on oriented cell divisions or expansions and create complex tissues by following local self-organizing feedback rules. Being rooted in the soil, plants are also highly adapted to cope with changing environments. Much of the adaptability and self-organization is mediated by the phytohormone auxin, with examples including the formation of an embryonic axis, regular arrangement of leaves and flowers on the stem, establishment of leaf venation, or flexible vasculature regeneration around a wound. Auxin also acts as a key endogenous signal positioning sessile plants in their environment during directional growth responses such as gravitropism and phototropism. Both self-organizing development and transla-

tion of environmental signals into directional growth rely on mechanistically elusive feedback between auxin signaling and polar auxin transport. 3,4

Directional cell-to-cell auxin transport is a plant-specific mechanism⁵ dependent upon plasma membrane-localized transporters. Ohief among these are AUX1/LAX importers and PIN auxin exporters. The latter inhabit polarized plasma membrane domains to determine vectorial auxin fluxes through tissues. Inside cells, auxin triggers a well-studied transcriptional pathway through predominantly nuclear TIR1/AFB receptors. This leads to developmental reprogramming auxin responses showed such rapidity that transcriptional cascades did not suffice for their explanation. While some of these were later found to also depend on TIR1/AFB receptors, others require extracellular (apoplastic) auxin perception. This has been formalized as comprising



⁶These authors contributed equally

⁷Lead contact





AUXIN-BINDING PROTEIN1 (ABP1), ABP1-LIKEs (ABLs), and TRANSMEMBRANE KINASEs (TMKs) (ABP1/ABL-TMK) co-receptor complexes at the cell surface. 15-17

Sensitive phospho-proteomic pipelines recently revealed that auxin triggers a global phosphorylation response via ABP1 and TMK1. ^{17,18} Notably, the lack of auxin-induced phosphorylation in *abp1* and *tmk1* mutants correlates with strong defects in auxin canalization, ¹⁷ a mysterious process underlying self-organizing plant development, including regeneration of vasculature and formation of polarized auxin-transporting channels from a local auxin source. Canalization also requires TIR1/AFB receptors, ¹⁹ suggesting that both intracellular and apoplastic signaling contribute to auxin feedback regulation of PIN-dependent auxin transport. This is consistent with computational predictions exploring the potential mechanism of PIN polarization by auxin feedback²⁰; however, no such mechanism linking auxin signaling and transport has been discovered.

Feedback between auxin and its transport has also been proposed for gravitropic root bending. Contrary to canalization, this would not involve adjustments of PIN polarity but rather the stabilization of the root-specific PIN2 transporter.²¹ Among the latest novelties in the quest of plants to grow upright is the evolution of fast root gravitropism, which was enabled by functional innovations in the PIN2 protein.²² Fast gravitropism occurs through directional auxin transport from the site of gravity perception toward the elongation zone where growth response takes place. After gravity sensing in the columella at the root tip,²³ auxin flux becomes redirected to the lower root side.^{24,25} This initial asymmetry is then propagated by AUX1- and PIN2-mediated transport^{26,27} from the root tip to the elongation zone and translated into root bending through local inhibition of cell elongation.²⁸

During the gravitropic response, PIN2 distribution itself becomes asymmetric with increased and decreased PIN2 stability at the lower and upper root sides, respectively. Such a lateral PIN2 gradient not only propagates but also reinforces the initial root tip auxin asymmetry, contributing to the robustness of root bending as well as to the fine-tuning of gravitropism by other hormonal cues. How auxin regulates its own transport via PIN2 in the context of root gravitropism remains an outstanding question.

In search of a possible mechanism for the cell-surface auxin signaling effect on auxin transport, we mined the auxin-inducible, ABP1-TMK1-mediated phospho-proteome and identified enrichment of PINs with PIN2 as the main target. We find that an auxin-induced interaction of TMK1 with PIN2 and its phosphorylation are directly responsible for the PIN2 gradient that reinforces gravitropic root bending. This pathway perceives auxin through the root-expressed ABL3 receptor, acting redundantly with ABP1. Our findings identify a direct mechanism for feedback regulation between auxin signaling and auxin transport.

RESULTS

ABP1-TMK1 cell-surface auxin signaling induces phosphorylation of PIN auxin transporters

To identify components of feedback regulation of auxin transport downstream of ABP1-TMK1 auxin signaling, we took advantage of a rapid phospho-proteomic dataset (100 nM indole 3-acetic acid [IAA], 2 min) recorded in roots of *Arabidopsis thaliana* (*Arabidopsis*) wild type (WT) or the respective mutants.¹⁷ We queried proteins concurrently hypo-phosphorylated in both *abp1-TD1* and *tmk1-1* mutants for molecular function using a Gene Ontology (GO) analysis. When partitioned by significance, the most dominant terms were rather general and included "binding" or "protein binding." On the other hand, partitioning significant terms by effect size (fold enrichment) always recovered "auxin efflux transmembrane transporter activity" as the most strongly enriched GO term (Figures S1A and S1B). Inspection of the corresponding enriched phospho-proteins showed the presence of PINs and ABCB/ABCG transporters. We further focused on PINs as dominant auxin transporters with many established developmental roles.

There were in total nine PIN phospho-peptides (phosphosites) significantly downregulated in both abp1-TD1 and tmk1-1 (Figures 1A and S1C). To verify the genetic specificity of these results, we examined in parallel a recent matched auxin phosphorylation dataset¹⁸ from the mutant of the intracellular AFB1 auxin receptor. 31 Except for PIN1 S337, none of the ABP1-TMK1-dependent PIN phospho-sites were deregulated in afb1-3 (Figure 1A). This suggests that auxin activates PIN phosphorylation specifically through the cell-surface ABP1-TMK1 module independently of intracellular TIR1/AFB signaling. Two of the nine PIN phospho-sites mapped to PIN1, five to PIN2, and two to PIN3 (Figure 1A). Notably, all these sites targeted hydrophilic PIN loops, the expected location for post-translational modifications regulating PIN function.³² The two PIN1 sites, PIN1^{S271} and PIN1^{S337}, were previously ascribed to shoot functions as targets of the D6PK protein kinase³³ and the MKK7-MPK6 module, 34 respectively. Another previously studied phospho-site was PIN2^{S439}, which participates in root adaptation to varying nitrogen sources. 35,36

Given that cell-surface auxin signaling mutants show perturbed phospho-proteomes even under mock conditions, 17,18 we next assessed auxin inducibility of these phospho-sites in WT roots. Notably, four out of five PIN2 phospho-sites strongly responded to 100 nM IAA within 30 s of treatment (Figure 1B). The PIN3^{S389} phospho-site showed a similar behavior. Conversely, while the auxin profile of PIN1^{S337} also significantly deviated from mock conditions, the site only underwent a delayed negative fluctuation (Figure S1D). This correlates with PIN1^{S337} not being specifically targeted by ABP1-TMK1 (Figure 1A). We also confirmed average to low evolutionary conservation of PIN1^{S337} (Figure S1E), altogether suggesting minor biological relevance of this particular site for the ABP1-TMK1 auxin phospho-response. When extending evolutionary conservation analysis to the remaining PIN phospho-sites, we observed moderate conservation of PIN1 S271 and poor conservation of the auxin-inducible PIN3S389 (Figures S1E and S1F). On the other hand, four out of five PIN2 phospho-sites showed high ConSurf scores and perfect conservation in PIN2 orthologs from Arabidopsis to gymnosperms (Figures 1C and 1D).

Given that rapid auxin phospho-response represents an ancient auxin pathway, ¹⁸ we next asked whether PIN phosphorylation is conserved across the green lineage. Unlike in *Arabidopsis*, we found no significantly regulated PIN phospho-sites in the auxin phospho-proteomes (100 nM IAA, 2 min) of two





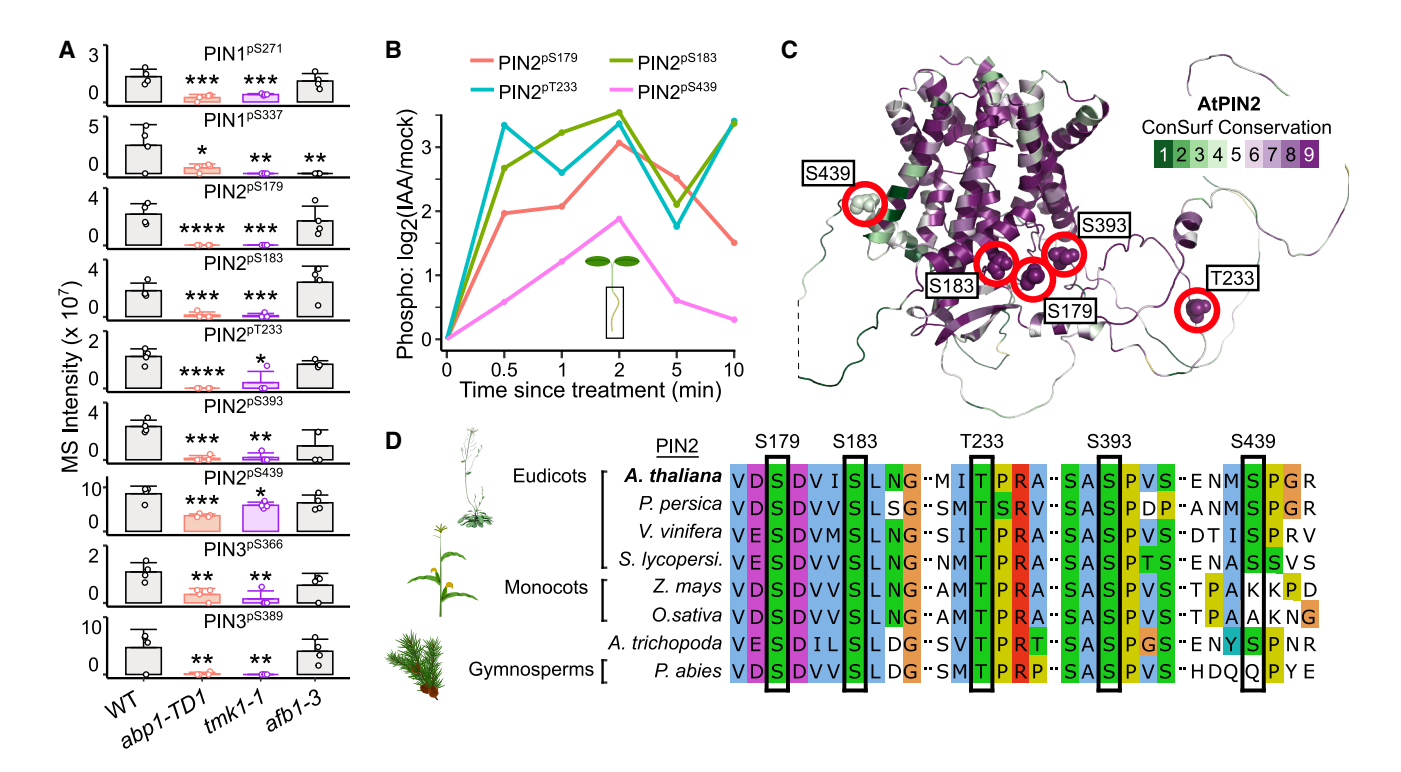


Figure 1. Rapid auxin phospho-response targets PINs in Arabidopsis

(A) Overview of PIN phospho-sites downregulated (false discovery rate [FDR] < 0.05) in abp1-TD1, tmk1-1, and afb1-3 auxin-treated (100 nM IAA, 2 min) roots. 4 biological replicates, mean + SD, permutation-based t tests with FDR-controlled p values. *p < 0.05, **p < 0.01, ***p < 0.001, ***p < 0.0001.

- (B) Significant PIN2 phospho-site auxin profiles (FDR \leq 0.01, 100 nM IAA).
- (C) Localization of ABP1-TMK1-dependent phospho-sites on a ConSurf conservation-colored AlphaFold2 structure of PIN2.
- (D) Multiple sequence alignment of eight PIN2 orthologs with a highlight of *Arabidopsis* ABP1-TMK1-dependent PIN2 phospho-sites. See also Figure S1.

bryophytes (*Physcomitrium* and *Marchantia*) and three streptophyte algae (*Penium*, *Chara*, ³⁷ and *Klebsormidium*). Conversely, the fern *Ceratopteris* showed auxin-regulated PIN phosphorylation under the same conditions. ³⁸ This suggests a co-option of an ancestral auxin response for PIN phosphorylation after the divergence of Bryophyta from the green lineage, probably in the common ancestor of vascular plants.

Our analyses thus identified PIN auxin transporters, particularly PIN2, as prominent targets of ultrafast ABP1-TMK1-mediated auxin phospho-response, representing a recent evolutionary innovation.

ABP1-TMK1-dependent PIN2 phospho-sites are crucial for PIN2 stability and root gravitropism

In further investigations, we focused on PIN2, as it was most extensively targeted, its phosphorylation strongly responded to auxin, and it showed remarkable conservation at the majority of its phospho-sites.

To test the physiological relevance of ABP1-TMK1-dependent PIN2 phosphorylation, we mutated the five candidate phospho-sites (Figures 2A and 2B) to either aspartate or alanine and introduced the resultant phospho-variants in the agravitropic eir1-4 mutant²¹ under the native PIN2 promoter. This yielded PIN2::PIN2^{WT}-GFP;eir1-4 (PIN2^{WT}-GFP), PIN2::PIN2^{5-MIMIC}-GFP;eir1-4 (PIN2^{5-MIMIC}-GFP), and PIN2::

PIN2^{5-DEAD}-GFP;eir1-4 (PIN2^{5-DEAD}-GFP). Given the rapidity of the auxin effect on PIN2 phosphorylation (Figure 1B), we specifically focused on early stages of gravitropic root bending. While PIN2WT-GFP complemented eir1-4 close to WT levels, the phospho-mimic PIN25-MIMIC-GFP provided only partial rescue (Figure 2C), an effect highly reproducible among independent lines. The phospho-dead PIN25-DEAD-GFP showed a weaker effect, which was pronounced during the first 2 h of bending and then slowly dissipated (Figure 2C). Interestingly, the PIN25-MIMIC-GFP phenotype extended beyond early gravitropic stages and was apparent even 12 h after gravistimulation (Figure S2A), suggesting that chronic ABP1-TMK1-like phosphorylation of PIN2 strongly perturbs root gravitropism. These results collectively demonstrate the importance of ABP1-TMK1-dependent phospho-sites for the physiological function of PIN2 in root gravitropism.

Phosphorylation of PIN2 by AGC3 kinases at PIN2^{S237}, PIN2^{S258}, and PIN2^{S310} was previously established as regulating polar PIN2 localization.³⁹ However, the five ABP1-TMK1-dependent PIN2 phospho-sites were non-overlapping (Figure 2A). Indeed, we observed stereotypical polarity of apical PIN2 in epidermal cells and basal PIN2 in young cortical cells in our *PIN2*^{5-MIMIC}-*GFP* and *PIN2*^{5-DEAD}-*GFP* phospho-lines (Figure S2B). While the PIN2 phospho-lines showed no obvious

Cell Article



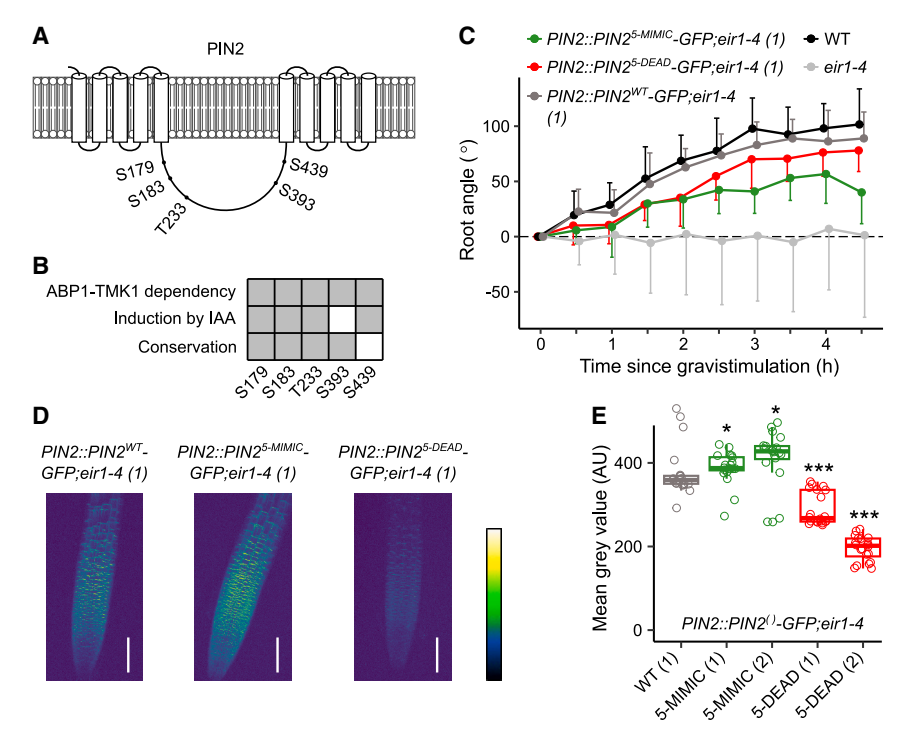


Figure 2. ABP1-TMK1-dependent PIN2 phospho-sites for gravitropism and PIN2 stability

(A) Schematic of ABP1-TMK1-dependent phospho-sites mapped on the PIN2 hydrophilic loop.(B) Schematic summarizing properties of the studied PIN2 phospho-sites.

(C) Root gravitropism of PIN2-GFP phospholines on medium with sucrose (1%). Mean \pm SD. (D) Representative maximum intensity projection images of PIN2-GFP phospho-lines. Scale bars, 100 μ m.

(E) Quantification of GFP signal from (D). Kruskal-Wallis analysis followed by Holm-corrected Wilcoxon rank sum tests relative to WT. *p < 0.05, **p < 0.01, ***p < 0.001, ****p < 0.0001. a.u., arbitrary units.

See also Figure S2.

polarity defects, we did observe reproducible differences in their GFP signal intensity. These were stronger than insertion-dependent variation when selecting T1 transformants and were also apparent in independent, single-insert, GFP-positive phospho-lines (Figure 2D). The $PIN2^{5-MIMIC}$ -GFP variants showed occasional weak stabilization compared with $PIN2^{WT}$ -GFP (Figures 2D and 2E). On the other hand, $PIN2^{5-DEAD}$ -GFP lines showed a highly consistent strong destabilization compared with $PIN2^{WT}$ -GFP roots (Figures 2D and 2E). Isolation of lines with comparable transgene mRNA levels unequivocally ruled out insertion-dependent expression artifacts and established the loss-of-phosphorylation stability defect as post-transcriptional (Figures S2C and S2D).

Altogether, our results show the relevance of ABP1-TMK1-dependent PIN2 phospho-sites for steady-state PIN2 stability and root gravitropism, suggesting a role of cell-surface auxin signaling in these processes.

Root-expressed ABL3 auxin receptor acts redundantly with ABP1 in root gravitropism

Next, we investigated the genetic basis of PIN2 phosphorylation by cell-surface auxin signaling. It recently became recognized that apoplastic auxin perception shows multi-level redundancy. 40,41 This includes a presumably abundant pool of poorly understood ABP1/ABL auxin receptors communicating with four possible TMKs, together activating global phosphorylation reprogramming of the cellular proteome. 15,17,18 Although we identified PINs as major phospho-targets of this signaling pathway (Figure 1A), the precise composition and redundancy of the upstream auxin signaling complexes remain elusive.

TMKs form a redundant family, with single mutants having rather subtle phenotypes and higher-order mutants showing strong de-

fects in growth and development.⁴² To study TMK expression in roots, we used global transcriptomic data and generated *TMK1::GUS*, *TMK2::GUS*, *TMK3::GUS*, and *TMK4::GUS* lines reporting the corresponding promoter activities. The dominant family member highly expressed in

roots was *TMK1*, followed by *TMK3* and *TMK4* with lower expression levels (Figures S3A–S3C). To examine the role of TMK1 in root gravitropism, we performed sensitive phenotyping of the qPCR-validated *tmk1-1* mutant (Figures S3D and S3G). This revealed an early root-bending defect that was complemented by a *TMK1::gTMK1-GFP* construct (Figure S3G). These data support TMK1 as the dominant TMK upstream of PIN2 phosphorylation.

Unlike *tmk1-1*, the well-established *abp1* mutant lines (*abp1-C1* and *abp1-TD1*) do not show any appreciable defects in gravitropism. ⁴³ Nevertheless, complementation of *abp1-TD1* by native expression of an auxin-binding-deficient ABP1 variant exerts a dominant-negative effect on root gravitropism, indicating the existence of unknown redundant ABLs interacting with TMK1 in the root. ¹⁵ A recent report ¹⁵ described the redundant action of ABP1 with two auxin receptors, ABL1 and ABL2. The *abp1;abl1;abl2* triple mutant shows normal gravitropism, however, consistent with the predominantly shoot-specific expression of *ABL1* and *ABL2* (Figure S3F).

Sensitive gravitropic phenotyping led us to identify a T-DNA insertion knockout of an ABL1/ABL2 paralog, which we named ABL3. The qPCR-validated (Figure S3E) abl3-1 mutation phenocopied the early root gravitropism defects of tmk1-1 but only in a double-mutant constellation with either abp1-C1 (Figures 3A and 3B) or abp1-TD1 (Figures 3B and S3H). The double-mutant phenotype was reproduced with an independent qPCR-validated (Figure S3E) T-DNA insertion line, abl3-2 (Figure S3I). We confirmed ABL3 (AT4G14630) expression in the root by mining public RNA sequencing (RNA-seq) data and using an ABL3::GUS line (Figures 3C and S3F). The ABL3 protein encompasses 222 residues and does not harbor a KDEL endoplasmic reticulum retention sequence. Superimposition of the Arabidopsis ABL3 AlphaFold2 structure with the





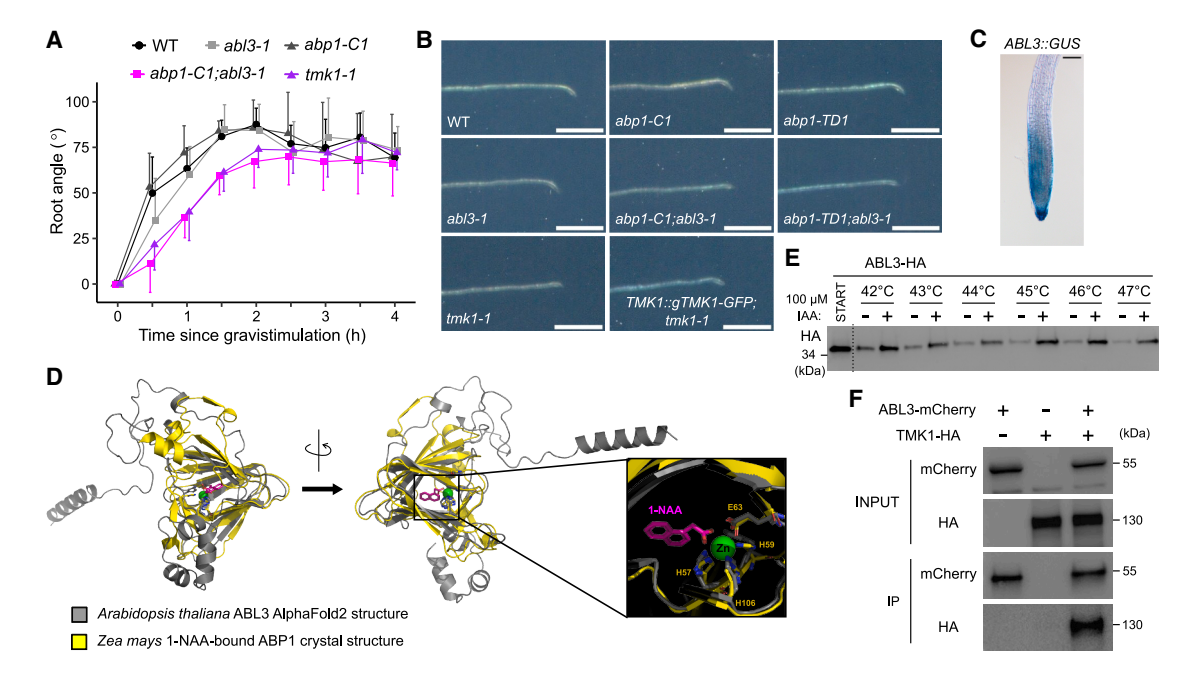


Figure 3. ABP1/ABL3-TMK1 signaling during early root gravitropism

- (A) Mutant root gravitropism profiles on medium without sucrose. Mean \pm SD.
- (B) Representative images of roots from (A) gravistimulated for 1 h. For the remainder of the corresponding quantifications, refer to Figures S3G and S3H. Scale bar, 1 mm.
- (C) ABL3::GUS staining (2 h). Scale bar, 100 μm.
- (D) Superimposition of the Arabidopsis ABL3 AlphaFold2 structure with the 1-NAA-bound maize ABP1 crystal structure highlighting a potential auxin-binding cavity of Arabidopsis ABL3.
- (E) CETSA-based binding assay for protection from thermal denaturation on 35S::ABL3-HA Arabidopsis root protoplasts in the presence of 100 µM IAA.
- (F) Co-immunoprecipitation (coIP) from tobacco leaves of TMK1-HA with ABL3-mCherry but not with anti-mCherry beads alone. See also Figure S3.

1-naphthaleneacetic acid (1-NAA)-bound maize ABP1 crystal structure revealed a potential auxin-binding cleft in AtABL3 (Figure 3D). This also highlighted that ABL3 conforms to the ancient cupin fold of ABP1. 44 Importantly, ABL3 showed perfect conservation of three metal-coordinating residues known to be indispensable for auxin binding in ABP1, ABL1, and ABL2 (Figure 3D). The sequence surrounding these residues resembled ABL1 and ABL2 more than ABP1 (Figure S3L), as expected from members of the same GERMIN-LIKE PROTEIN (GLP) family. 16

Next, we tested whether ABL3 binds auxin using a cellular thermal shift assay (CETSA) followed by western blotting. The natural auxin IAA conferred protection from thermal denaturation on ABL3-HA in protein extracts from *Arabidopsis* root protoplasts transformed with 35S::*ABL3-HA* (Figure 3E). Likewise, IAA protected ABL3-6xHIS-3xFLAG (or ABL3-HF) in protein extracts from *Arabidopsis* seedlings stably transformed with 35S:: *ABL3-HF* (Figure S3J). These results qualify ABL3 as an auxin-binding protein.

To transmit signals from auxin-bound ABL3, TMK1 would be expected as an ABL3 interaction partner. Indeed, in tobacco leaves, TMK1-HA co-immunoprecipitated with ABL3-mCherry but not with anti-mCherry beads alone (Figure 3F). Reciprocally, we further confirmed this interaction in *Arabidopsis* root protoplasts, where ABL3-HA co-immunoprecipitated with TMK1-mCherry but not with anti-mCherry beads alone (Figure S3K).

Thus, we identified ABL3 as a root-expressed auxin-binding protein interacting with TMK1 and acting redundantly with ABP1 in root gravitropism. These observations are consistent with the notion that the cell-surface ABP1/ABL3-TMK1 module represents a root-specific pathway targeting PIN2 phosphorylation for early stages of gravitropic root bending.

Exogenous and endogenous auxin activate TMK1 and downstream ROP signaling in roots

Despite recent progress, the cellular and molecular readouts of cell-surface TMK1-dependent auxin signaling remain poorly established. Previous data showed that the cytoplasmic part of TMK1 harbors an ABP1-dependent phospho-site. Teurthermore, the TMK1 kinase domain shows a capacity to auto-phosphorylate, and research on other leucine-rich repeat receptor-like kinases (LRR-RLKs) suggests that phosphorylation of their cytoplasmic domains leads to LRR-RLK activation. A6,47

Therefore, we examined TMK1 phosphorylation in response to auxin. We immunoprecipitated TMK1-FLAG from auxin-treated (IAA, 10 nM, 1 h) *TMK1::TMK1-FLAG;tmk1-1* roots. After confirming successful immunoprecipitation (IP) with an anti-FLAG antibody, we stripped and re-probed the membranes with a Phos-tag Biotin Probe that coordinates tetrahedral phosphate moieties. We observed significant induction of TMK1





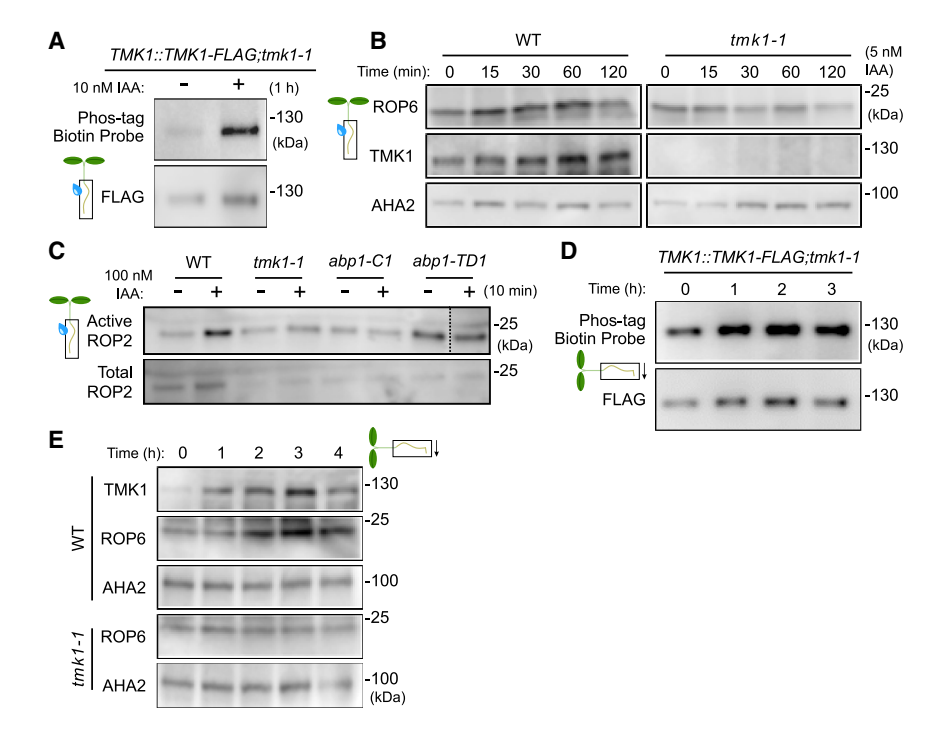


Figure 4. Auxin-induced activation of TMK1 and downstream ROP signaling in roots

(A) Auxin effect on TMK1 phosphorylation in *TMK1:: TMK1-FLAG;tmk1-1* roots assayed through TMK1-FLAG IP and Phos-tag Biotin Probe analysis. Refer to Figure S5A for quantification of three experimental replicates.

(B) Auxin effect on ROP6 and TMK1 levels in the WT or *tmk1-1* root microsomal protein fractions. Refer to Figure S5B for quantification of three experimental replicates.

(C) Auxin effect on ROP2 activation assayed by native ROP pull-down from roots of the indicated genotypes. The empty well was edited out from the upper blot for visualization purposes. Refer to Figure S4D for the unedited blot image.

(D) Gravistimulation effect on TMK1 phosphorylation in *TMK1::TMK1-FLAG;tmk1-1* roots assayed through TMK1-FLAG IP and Phos-tag Biotin Probe analysis. Refer to Figure S4F for quantification of three experimental replicates.

(E) Gravistimulation effect on ROP6 and TMK1 levels in the WT or *tmk1-1* root microsomal protein fractions. Refer to Figure S4G for quantification of three experimental replicates.

See also Figure S4.

phosphorylation by auxin, presumably corresponding to increased TMK1 activity (Figures 4A and S4A).

As a downstream response, we investigated the root-specific activation of small GTPases from the RHO OF PLANTS (ROP) family implicated downstream of ABP1/ABL-TMKs. Previous ROP activation assays relied extensively on ROP overexpression, used the synthetic auxin 1-NAA, and were usually performed with leaf tissue. 15,48,49 We specifically asked if the natural auxin IAA activates ROPs in roots under non-overexpressing conditions. Immunoblotting microsomal protein extracts from auxin-treated (IAA, 5 nM, 0-120 min) roots with an anti-ROP6 antibody revealed auxin-induced enrichment of ROP6 in WT but not in tmk1-1 (Figures 4B and S4B). Given that membrane association is a prerequisite for ROP activation, 50 enrichment in the microsomal fraction likely reports TMK1-dependent ROP6 activation by auxin. Interestingly, we also observed that auxin stabilized TMK1 itself (Figures 4A, 4B, and S4B) but did not induce TMK1 mRNA over time (IAA, 10 or 100 nM, 0-120 min; Figure S4C). Such TMK1 stabilization at the membrane might be related to the recently reported auxin-mediated TMK1 nano-clustering effect.51

We next used an orthogonal method to study ROP activation by auxin. As usual for small GTPases, only GTP-bound (active) but not GDP-bound (inactive) ROP proteins engage in protein-protein interactions with their effectors. We purified the Cdc42/Rac-interactive binding motif (CRIB) domain of the RIC1 ROP effector from bacteria and used it to pull down active ROPs from native root protein extracts. Immunoblotting with an anti-ROP2 antibody revealed a strong auxin-induced (IAA, 100 nM, 10 min) ROP2 activation in WT but much weaker activation in tmk1-1, abp1-C1, or abp1-TD1 roots (Figures 4C and S4D). This confirms that auxin in roots activates ROP2 through the ABP1-TMK1 module.

To test whether the above observations remain valid also when auxin levels are changed endogenously, we repeated TMK1-FLAG IP followed by a Phos-tag Biotin Probe blotting on gravistimulated roots. This revealed a significant increase in TMK1 phosphorylation (Figures 4D and S4F), indicating that gravistimulation activates TMK1. Accordingly, gravistimulation also induced a TMK1-dependent enrichment of ROP6 in the microsomal fraction (Figures 4E and S4G).

Overall, these data show that both exogenous and endogenous elevations of auxin levels promote TMK1 phosphorylation and activation of downstream ROP GTPase signaling.

Asymmetric activation of TMK1 and downstream ROP signaling in root gravitropism

Having established auxin-induced TMK1 activation in the root (see Figures 4 and S4) and the importance of ABP1-TMK1-dependent PIN2 phosphorylation for its stability and in early gravitropic root bending (see Figures 1, 2, S1, and S2), we assessed the role of these regulations in root gravitropism.

Our experiments with native ROP activation suggested auxinresponsive ROP signaling as a suitable proxy for TMK1 activity
in the root tissue (Figures 4 and S4). However, blotting-based assays do not provide sufficient spatiotemporal resolution. For this
reason, we constructed an *in situ* ROP sensor by inserting (1)
ROP2 and (2) the CRIB domain of the ROP effector RIC1 on opposite ends of a circularly permuted GFP (cpGFP). The cpGFP fluorescence should decrease when activated GTP-bound ROP2
interacts with the nearby CRIB domain (Figure S5D). Expression
of CRIB-cpGFP-ROP2 and mCherry-ROP2 from the same
cassette yielded a ratiometric ROP sensor, which we called the
cpGFP ROP activity probe (CRAP). As expected, the 561/
488 nm CRAP ratio sensitively reported auxin (IAA, 10 nM) pulses
in *CRAP;WT* roots in a microfluidic root chip setup (Figure S5E).





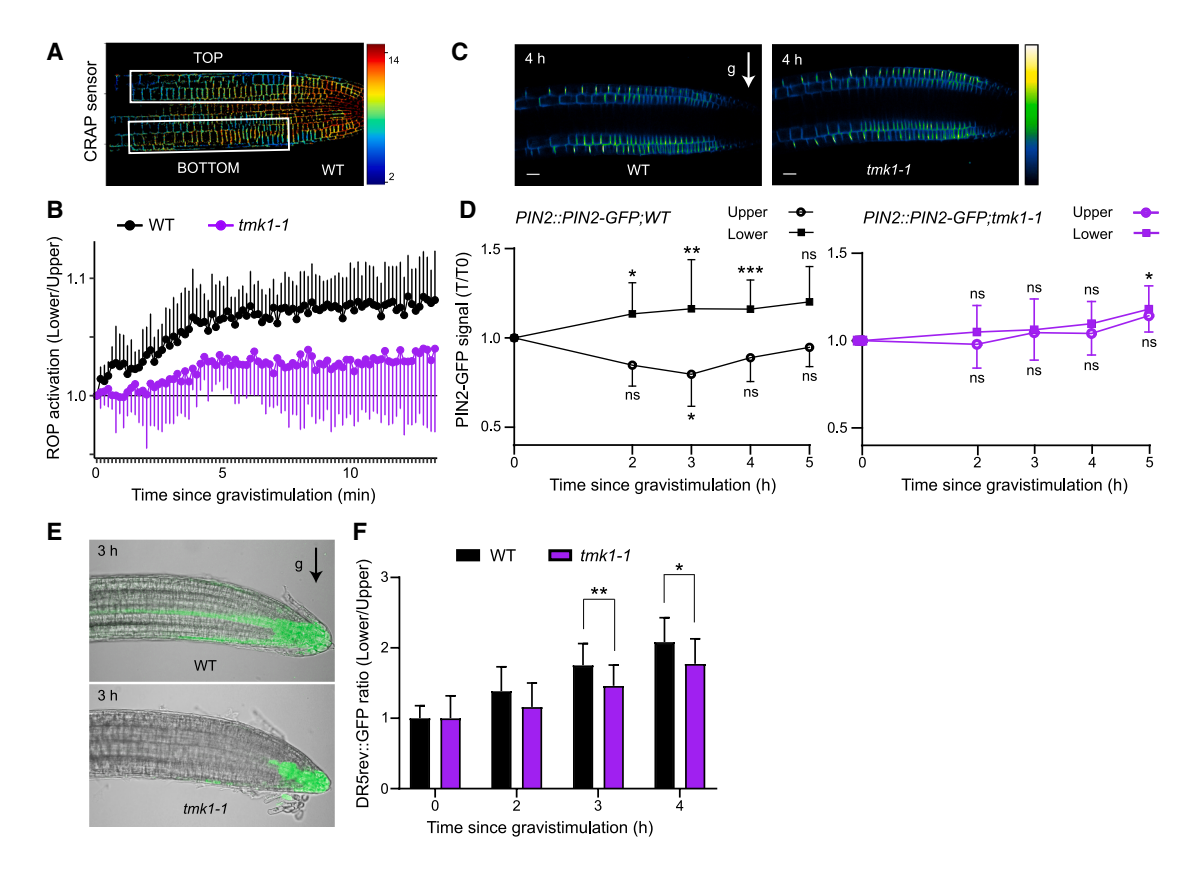


Figure 5. Asymmetric TMK1 activation for PIN2 asymmetry in root gravitropism

- (A) Image of a root with strongly asymmetric ROP activity (reported by the CRAP sensor) in response to 15-min gravistimulation.
- (B) Rapid gravistimulation-induced establishment of asymmetric ROP activity in WT or *tmk1-1* roots. Mean ± SD.
- (C) Representative images of PIN2::PIN2-GFP in 4-day-old WT and tmk1-1 seedlings after 4 h of gravistimulation. g, gravity vector. Scale bar, 20 µm.
- (D) Quantification of gravistimulation-induced PIN2-GFP asymmetry. Normalization was to the respective first time point (T0) for the upper or lower root side. Mean \pm SD. Two-way ANOVA with Dunnett's multiple comparisons, *p < 0.05, **p < 0.01, ***p < 0.001, ****p < 0.0001.
- (E) Representative confocal images of asymmetric auxin response (visualized by *DR5rev::GFP*) at the lower side of the root after a 3-h gravistimulation in WT and *tmk1-1* 4-day-old roots. Refer to Figure S6H for corresponding images taken before gravistimulation. *g*, gravity vector.
- (F) Quantification of *DR5rev::GFP* asymmetry as a ratio of fluorescence intensity at the lower side to the upper side of gravistimulated roots at the indicated time points, normalized to the initial fluorescence value. Mean + SD, n = 10. Two-way ANOVA with Dunnett's multiple comparisons, *p < 0.05, **p < 0.01. See also Figure S5.

Notably, within 5 min of gravistimulation, CRAP-expressing roots developed an asymmetric pattern with significantly more ROP activation at the lower side of the root (Figure 5A). A GDP-locked CRAP (CRIB-cpGFP-ROP2^{T20N}) failed to show this asymmetry, confirming that CRAP indeed reports ROP activation rather than, e.g., local fluctuations of the cpGFP root microenvironment (Figure S5F). This identifies an asymmetric rapid response to gravity-induced auxin flux redirection in roots, as confirmed by the lack of CRAP asymmetry after inhibition of auxin transport by naphthylphthalamic acid (NPA) (Figure S5I).

Given that auxin-induced ROP activation is TMK1-dependent (Figures 4 and S4), the gravitropic CRAP gradient likely mirrors asymmetric TMK1 activation by auxin flow from the root tip. Indeed, the *tmk1-1* background abolished asymmetric ROP activation in *CRAP;tmk1-1* roots (Figure 5B). These data collectively establish rapid asymmetric activation of the TMK1 kinase and downstream ROP signaling by redirection of auxin fluxes during gravitropic root bending.

Asymmetric TMK1 activation correlates with PIN2 asymmetry in root gravitropism

The rapid TMK1 activation along the lower root side corresponds well with the time frame in which auxin induces PIN2 phosphorylation through TMK1 (Figure 1B), inferring that asymmetric TMK1 activation likely results in asymmetric PIN2 phosphorylation. Given that TMK1-regulated phospho-sites mediate PIN2 stability (see Figure 2), we decided to follow the fate of PIN2-GFP in gravistimulated roots. We observed asymmetric PIN2-GFP stabilization at the lower root side, as shown before, 21,29,52 and this was completely abolished in the *tmk1-1* mutant (Figures 5C and 5D).

We further assessed the role of TMK1 and its kinase activity by cloning a kinase-dead TMK1 construct carrying a mutation in the ATP-binding site and generating *UBQ10::TMK1*^{K616R}-mCherry (TMK1^{DN}) in a WT background. Notably, TMK1^{DN} expression perturbed the gravity-induced PIN2-GFP asymmetry (Figure S5G). Accordingly, it also conveyed an early defect in gravitropic root bending (Figures S5A and S5B), phenocopying the *tmk1-1* mutant





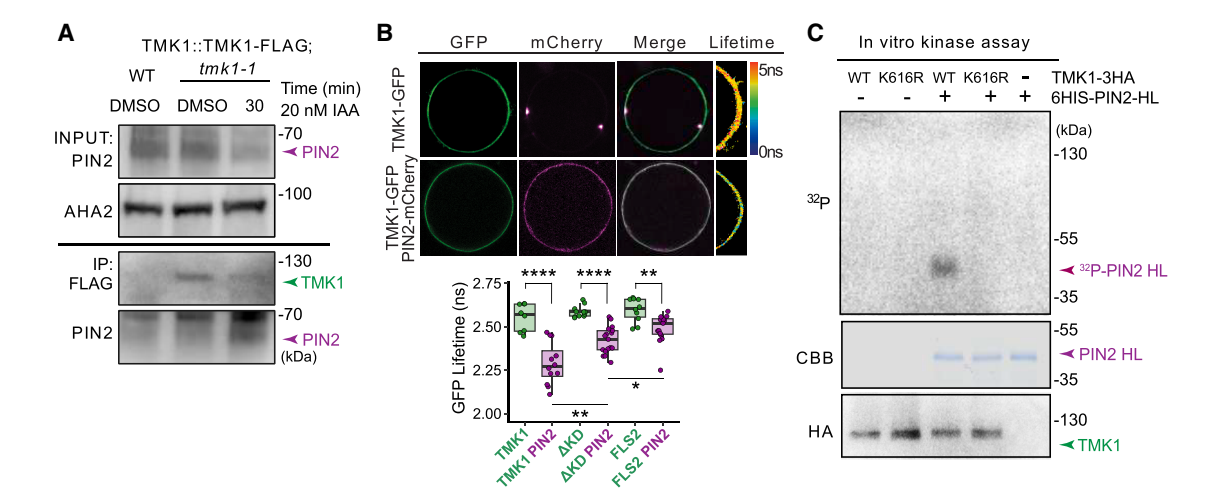


Figure 6. Auxin-mediated TMK1 interaction with and phosphorylation of PIN2

(A) Auxin promotes the interaction between TMK1 and PIN2 in a coIP assay. Microsomal protein fraction from 20 nM IAA- or DMSO-treated *TMK1::TMK1-FLAG; tmk1-1* roots was immunoprecipitated with an anti-FLAG antibody, and endogenous PIN2 was detected by blotting with an anti-PIN2 antibody. The microsomal protein fraction from WT was used as a control for nonspecific binding of endogenous PIN2.

(B) FRET-FLIM analysis on transiently expressed 35S::TMK1-GFP, 35S::TMK1-GFP, 35S::FLS2-GFP, and 35S::PIN2-mCherry in root protoplasts. Fluorescence lifetime values are displayed as a heatmap (for the remaining images, see Figure S6C). One-way ANOVA with Holm-corrected post hoc t tests, *p < 0.05, ****p < 0.0001.

(C) In vitro kinase assay showing that TMK1-3xHA directly phosphorylates the 6His-PIN2 HL. Top, ³²P autoradiography; middle, Coomassie brilliant blue (CBB) staining; bottom, immunoblot with an anti-HA antibody. See also Figure S6.

(Figures 3A and S3G). The TMK1^{DN}-expressing plants showed unperturbed levels of the endogenous TMK1 protein (Figure S5C), ruling out transgene-induced silencing of the endogenous *TMK1* gene. This shows that TMK1^{DN} causes a dominant-negative phenotype, underscoring the importance of TMK1 kinase activity for both gravity-induced PIN2 asymmetry and rapid bending response.

The requirement of TMK1 for the PIN2-GFP gradient suggests that TMK1 stabilizes PIN2 to enhance PIN2-mediated auxin flux from the root tip along the lower root side. To test this, we monitored the DR5rev::GFP auxin response reporter, which revealed a significantly decreased gravity-induced auxin asymmetry in tmk1-1 compared with WT (Figures 5E, 5F, and S5H). Accordingly, inhibition of PIN-mediated auxin transport by NPA interfered not only with CRAP-reported asymmetric TMK1 activation (Figure S5I) but also with the PIN2-GFP asymmetry (Figure S5J), confirming that polar auxin transport itself contributes to asymmetric TMK1 activation and subsequent PIN2 stabilization for further asymmetric auxin flow reinforcement. Finally, we followed PIN2-GFP gradient formation in the abp1-TD1;abl3-1 background, which revealed a perturbed profile that was especially deficient in the maintenance phase (Figure S5K). The residual PIN2-GFP asymmetry contrasts with the complete abolishment in tmk1-1 and likely indicates the existence of further unexplored ABL proteins upstream of TMK1.

Altogether, these data identify a positive feedback loop in which, following gravistimulation, PIN2 redistributes auxin from the root tip to the lower root side, activating the TMK1 kinase, which promotes PIN2 phosphorylation and stabilization, channeling even more auxin along the lower root side and reinforcing the original gravity-induced auxin flow asymmetry.

Auxin induces TMK1 interaction with PIN2 and phosphorylation of its hydrophilic loop

Our hitherto results demonstrate a strong functional relevance of TMK1-dependent PIN2 phosphorylation during root gravitropism. Co-localization of TMK1-GFP and PIN2-mCherry expressed from native promoters suggested a possibility for their direct interaction (Figure S6A). To test this, we immunoprecipitated TMK1-FLAG from *TMK1::TMK1-FLAG;tmk1-1* roots and used an anti-PIN2 antibody for detection of native PIN2. PIN2 did not co-immunoprecipitate with TMK1-FLAG in untreated samples. On the other hand, in auxin-treated roots (IAA, 5 or 20 nM, 15 or 30 min), PIN2 co-immunoprecipitated with TMK1-FLAG in a time-dependent and auxin concentration-dependent manner (Figures 6A, S6B, S6E, and S6F). This suggests that auxin promotes the formation of a TMK1-PIN2 complex at the plasma membrane.

To verify the biochemical evidence for TMK1-PIN2 interaction, we performed fluorescence lifetime imaging on fluorescence resonance energy transfer (FRET)-pair-tagged proteins (FRET-FLIM), a technique that quantitatively reports protein interactions. We introduced 35*S::TMK1-GFP* and 35*S::PIN2-mCherry* in *Arabidopsis* root protoplasts and measured the fluorescence lifetime of the GFP signal. PIN2-mCherry strongly reduced the lifetime of TMK1-GFP, demonstrating an interaction between TMK1 and PIN2 (Figure 6B). Notably, a truncated TMK1^{ΔKD}-GFP variant without a kinase domain caused a significant drop in the interaction strength compared with TMK1-GFP. The interaction of an unrelated RLK FLS2-GFP with PIN2-mCherry was even weaker than that of TMK1^{ΔKD}-GFP (Figures 6B and S6C). These results establish both the contribution of the TMK1 kinase domain and the specificity of the TMK1-PIN2 interaction.





An auxin-induced TMK1-PIN2 interaction provides a plausible mechanism for the TMK1-dependent PIN2 phosphorylation observed in phospho-proteomic data (Figures 1 and S1). To test this, we performed an *in vitro* phosphorylation assay with ³²P-ATP as a phosphate donor. We incubated a purified N-terminally HIS-tagged PIN2 hydrophilic loop (HIS-PIN2-HL) with TMK1-3HA immunoprecipitated from a root protein extract. The results showed that intact TMK1-3HA but not the kinasedead version TMK1^{K616R}-3HA was able to phosphorylate HIS-PIN2-HL (Figure 6C). We did not observe any auxin effect in this kinase assay (Figure S6D), presumably due to saturation of TMK1-3HA activity by endogenous auxin during IP from TMK1-3HA roots.

Taken together, these data demonstrate that the RLK TMK1 interacts, in an auxin-dependent manner, with the PIN2 auxin efflux carrier and phosphorylates its HL.

DISCUSSION

Co-option of ancient auxin phospho-response for auxin feedback on its transport in vascular plants

Previous work indicated that while the rapid ABP1-TMK1-mediated auxin phospho-response is relevant for some rapid cellular auxin effects, specifically cytoplasmic streaming and apoplast acidification, ^{13,17,18,53} abp1 and tmk mutants also show severe phenotypes in the long-term establishment of auxin- and auxin transport-positive channels after wounding and from externally applied auxin sources, leading to vasculature formation. ¹⁷ The underlying mechanism of this so-called auxin canalization is largely unclear, but at its center lies feedback regulation between auxin signaling and directional auxin transport. ^{3,4}

Here, mining of a root ABP1-TMK1 phospho-proteome revealed PIN auxin transporters as major phospho-targets of the ABP1-TMK1 cell-surface auxin perception. It follows that PIN phosphorylation by ABP1-TMK1 likely modulates directional auxin transport to delineate auxin channels for subsequent vascular differentiation and eventually other processes involving feedback regulation of auxin transport. Consistently, a 15-yearold model predicted extracellular auxin perception as a key signaling input parameter for auxin canalization.20 Although the auxin phospho-response evolved in unicellular algae, 18 we find that it began targeting PINs only after the divergence of Bryophyta from the green lineage, likely in the common ancestor of vascular plants. The ABP1-TMK1-mediated PIN phosphorylation thus represents a recent evolutionary novelty that arose through the co-option of ancient rapid auxin response, presumably to enable the formation and regeneration of vasculature.

ABP1-TMK1-mediated phosphorylation encodes PIN2 stability

Focusing on the dominant phospho-target PIN2, we report five ABP1-TMK1-dependent phospho-sites, the majority of which are induced by auxin and remarkably conserved. Strikingly, neither of these overlaps with previously published polarity-regulating PIN2 phospho-sites.³⁹ Indeed, both PIN2 stability and the physiological function of PIN2 in root gravitropism require ABP1-TMK1-dependent phospho-sites, implying the existence of two PIN2 phospho-codes: one for stereotypical maintenance of

PIN2 polarity via AGC3 kinases³⁹ and the other for dynamic adjustments of PIN2 stability in response to auxin.

While loss-of-phosphorylation *PIN2-GFP*;*eir1-4* lines phenocopy the early root agravitropic phenotype of the *tmk1* mutant, gain-of-phosphorylation lines manifest a more severely perturbed gravitropic profile. This stronger phenotype might be a consequence of the PIN2 phospho-mimic protein showing excessive auxin transport rates, which would not be permissive to sufficient auxin accumulation at the lower root side during gravitropism.⁵⁴

ABL3: Root-expressed auxin receptor acting redundantly with ABP1 in root gravitropism

The overall lack of *tmk1*-like phenotypes in *abp1* mutants, despite the strong similarity of phospho-proteomic signatures between *abp1* and *tmk1*, ¹⁷ contributed to the historical controversy surrounding ABP1. Indeed, while we confirmed an early agravitropic phenotype in the *tmk1* mutant, *abp1* mutant alleles showed normal root bending, as reported before. ⁴³ Hidden genetic redundancy with distant but structurally conserved ABL proteins has been invoked to explain this discrepancy; however, the recently identified ABL1 and ABL2 show minimal expression in the root, and the *abp1;abl1;abl2* triple mutant shows normal gravitropism. ¹⁵

We identified the root-expressed ABL protein, ABL3, through genetic redundancy with ABP1 and as an auxin binder and TMK1 interactor. Notably, ABL3 is paralogous to both ABL1 and ABL2, as they all belong to the 32-member *Arabidopsis* GLP family, which is distantly related to ABP1 by the cupin fold. 44 ABP1 and ABL3 likely form part of an auxin-sensing complex docking on TMK1 in the root, providing a plausible model for auxin perception upstream of PIN2 phosphorylation.

While the field has so far only scratched the surface of the real diversity of potential cell-surface auxin receptors, this paints a picture in which specialized expression patterns of ABL auxin receptors confer specific functions on the rather ubiquitously expressed TMKs. There are likely more root-expressed ABLs awaiting discovery because *tmk1* and *abp1;abl3* mutants show a weaker phenotype than both the dominant-negative *ABP1: ABP1-5;abp1-TD1* line ¹⁵ and higher-order *tmk* mutants. ^{42,55}

Model for TMK1-based auxin feedback on PIN2mediated transport in root gravitropism

The PIN2 transporter evolved as a specific component of efficient root gravitropism in seed plants, ²² and it is well documented that its abundance during gravistimulation becomes asymmetric, with more PIN2 found at the lower root side. ^{21,29} This reinforces an initial auxin gradient and contributes to the robustness of root bending. ³⁰ Nonetheless, the molecular mechanism behind this regulation has remained unknown since its discovery almost 20 years ago. Here, the wealth of our data together argues for a model encompassing auxin feedback on its transport.

A change in the gravity vector is sensed in the root columella, which establishes an initial auxin flow redirection to the lower side of the root.²³ This initial auxin asymmetry activates the TMK1 kinase specifically at the lower root side. Activated TMK1 then interacts with PIN2 in the epidermis and phosphorylates its hydrophilic loop at several conserved stability-regulating phospho-sites, leading to PIN2 stabilization in these cells. The resulting PIN2 abundance gradient further enhances auxin





transport along the lower root side to the elongation zone, where it activates intracellular TIR1/AFB auxin signaling for growth inhibition and downward root bending. This demonstrates the existence of a positive feedback loop representing a direct molecular mechanism for auxin feedback on its transport.

The TMK-based auxin feedback regulation likely represents a more general mechanism acting in various developmental contexts with different PIN transporters, thereby mediating specialized aspects of adaptive and self-organizing plant growth and development. This is supported by the identification of TMK1-mediated PIN1 phosphorylation in the context of PIN polarity and auxin canalization. The TMK-PIN mechanism evolved recently in vascular plants through the co-option of an ancestral auxin phospho-response from unicellular algae, and it likely diversified to guide the auxin-mediated development of morphologically complex plants.

Limitations of the study

Our work establishes a phosphorylation-based feedforward loop between ABP1/ABL3-TMK1 cell-surface auxin signaling and PIN2-mediated polar auxin transport in root gravitropism. Importantly, the root-expressed ABL3 auxin receptor extends the concept of ABP1/ABL signaling to roots, mirroring hypocotyland pavement cell-centered functions of the dominantly shootexpressed ABL1 and ABL2 receptors. 15 Nevertheless, several lines of evidence indicate the existence of further unknown ABL proteins in the root. First, the gravitropic PIN2-GFP asymmetry is fully absent in tmk1 but partially persists in abp1;abl3 mutants. Second, tmk1 and abp1;abl3 mutants show weaker root growth and bending defects than both the dominant-negative ABP1::ABP1-5;abp1-TD1 line¹⁵ and higher-order tmk mutants. 42,55 Future studies should undertake a systematic effort to define which of the 32 Arabidopsis GLP proteins act as ABL auxin receptors. Finally, how PIN phosphorylation on specific residues downstream of different signaling pathways³² selectively affects PIN activity, polarity, or stability, remains a persistent mystery in the auxin transport field.

RESOURCE AVAILABILITY

Lead contact

Further information and requests for resources and reagents should be directed to and will be fulfilled by the lead contact, Jiří Friml (jirí.friml@ista.ac.at).

Materials availability

Constructs, genetic material, and reagents from this study are available from the lead contact upon request.

Data and code availability

- This work does not report original code.
- Phospho-proteomic and genomic analyses used publicly available datasets referenced in the main text and STAR Methods.
- Any additional information required to reanalyze the data reported in this
 paper is available from the lead contact upon request.

ACKNOWLEDGMENTS

We gratefully acknowledge Tongda Xu for experimental, material, and conceptual support. We thank William Gray for providing material, Nataliia Gnyliukh and Ema Cervenova for help with manuscript preparation, and Julia Schmid for help with cloning. We thank Dolf Weijers, Mark Roosjen, and Andre Kuhn

for discussions and support with phospho-proteomic analyses. We thank the Bioimaging and Life Science facilities at the Institute of Science and Technology Austria (ISTA) for their excellent service and assistance. The research leading to these results has received funding from the European Union (ERC, CYNIPS, 101142681) and Austrian Science Fund (FWF; I 6123-B) to J.F., and Y.J. was funded by ERC no. 3363360-APPL under FP/2007-2013. L.R. was supported by the FP7-PEOPLE-2011-COFUND ISTFELLOW program (IC1023FELL01) and the European Molecular Biology Organization (EMBO) long-term postdoctoral fellowship (ALTF 985-2016). S.T. was supported by the National Natural Science Foundation of China (32321001, 32570366). The work of J.H. was supported by the project JG_2024_003 implemented within the Palacký University Young Researcher Grant.

AUTHOR CONTRIBUTIONS

Conceptualization, J.F. and L.R.; methodology, L.R., L.F., and I.K.; investigation, L.R., L.F., M.Z., C.G., D.V., A.M., M.R., Y.Y., Z.G., I.V., J.H., M.C., S.T., L.H., L.L., M.M.M.-B., Z.Q., and G.M.; resources, L.R., L.F., M.M.M.-B., and Y.J.; writing, J.F., L.F., and L.R.; review and editing, all authors; visualization, L.R. and L.F.; supervision, J.F., L.F., and L.R.; and funding acquisition, J.F.

DECLARATION OF INTERESTS

The authors declare no competing interests.

STAR*METHODS

Detailed methods are provided in the online version of this paper and include the following:

- KEY RESOURCES TABLE
- EXPERIMENTAL MODEL AND STUDY PARTICIPANT DETAILS
 - Molecular cloning, plant material, and growth conditions
- METHOD DETAILS
 - o Bioinformatics
 - o RT-qPCR
 - o Fluorescence lifetime imaging
 - o GUS staining
 - Root gravitropic assays
 - o Imaging of transgenic lines
 - Microsomal protein extraction
 - o CETSA
 - o Western blot analysis of phosphorylated proteins
 - o Co-immunoprecipitation assays
 - o Active ROP assay on non-overexpressing plants
 - o Recombinant protein expression and purification from E. coli
 - o TMK1-HA immunoprecipitation
 - o In vitro kinase assay
 - Statistical analysis

SUPPLEMENTAL INFORMATION

Supplemental information can be found online at https://doi.org/10.1016/j.cell. 2025.08.026.

Received: November 29, 2022 Revised: February 17, 2025 Accepted: August 17, 2025 Published: October 2, 2025

REFERENCES

- Friml, J. (2022). Fourteen Stations of Auxin. Cold Spring Harb. Perspect. Biol. 14, a039859. https://doi.org/10.1101/cshperspect.a039859.
- Han, H., Adamowski, M., Qi, L., Alotaibi, S.S., and Friml, J. (2021). PIN-mediated polar auxin transport regulations in plant tropic responses. New Phytol. 232, 510–522. https://doi.org/10.1111/nph.17617.





- Berleth, T., and Sachs, T. (2001). Plant morphogenesis: Long-distance coordination and local patterning. Curr. Opin. Plant Biol. 4, 57–62. https:// doi.org/10.1016/S1369-5266(00)00136-9.
- Hajný, J., Tan, S., and Friml, J. (2022). Auxin canalization: From speculative models toward molecular players. Curr. Opin. Plant Biol. 65, 102174. https://doi.org/10.1016/J.PBI.2022.102174.
- Luschnig, C., and Friml, J. (2024). Over 25 years of decrypting PIN-mediated plant development. Nat. Commun. 15, 9904. https://doi.org/10.1038/s41467-024-54240-y.
- Luschnig, C., and Vert, G. (2014). The dynamics of plant plasma membrane proteins: PINs and beyond. Development 141, 2924–2938. https://doi.org/10.1242/dev.103424.
- Park, J., Lee, Y., Martinoia, E., and Geisler, M. (2017). Plant hormone transporters: what we know and what we would like to know. BMC Biol. 15, 93. https://doi.org/10.1186/S12915-017-0443-X.
- Péret, B., Swarup, K., Ferguson, A., Seth, M., Yang, Y., Dhondt, S., James, N., Casimiro, I., Perry, P., Syed, A., et al. (2012). AUX/LAX Genes Encode a Family of Auxin Influx Transporters That Perform Distinct Functions during Arabidopsis Development. Plant Cell 24, 2874–2885. https://doi.org/10. 1105/tpc.112.097766.
- Zhang, J., Nodzyński, T., Pěnčík, A., Rolčík, J., and Friml, J. (2010). PIN phosphorylation is sufficient to mediate PIN polarity and direct auxin transport. Proc. Natl. Acad. Sci. USA 107, 918–922. https://doi.org/10.1073/ pnas.0909460107.
- Wisniewska, J., Xu, J., Seifertová, D., Brewer, P.B., Růžička, K., Blilou, I., Rouquié, D., Benková, E., Scheres, B., and Friml, J. (2006). Polar PIN localization directs auxin flow in plants. Science 312, 883. https://doi.org/10. 1126/science.1121356.
- Prigge, M.J., Platre, M., Kadakia, N., Zhang, Y., Greenham, K., Szutu, W., Pandey, B.K., Bhosale, R.A., Bennett, M.J., Busch, W., et al. (2020). Genetic analysis of the Arabidopsis TIR1/ AFB auxin receptors reveals both overlapping and specialized functions. eLife 9, e54740. https://doi.org/10.7554/eLife.54740.
- Qi, L., Kwiatkowski, M., Chen, H., Hoermayer, L., Sinclair, S., Zou, M., Del Genio, C.I., Kubeš, M.F., Napier, R., Jaworski, K., et al. (2022). Adenylate cyclase activity of TIR1/AFB auxin receptors in plants. Nature 611, 133–138. https://doi.org/10.1038/s41586-022-05369-7.
- Li, L., Verstraeten, I., Roosjen, M., Takahashi, K., Rodriguez, L., Merrin, J., Chen, J., Shabala, L., Smet, W., Ren, H., et al. (2021). Cell surface and intracellular auxin signalling for H+ fluxes in root growth. Nature 599, 273–277. https://doi.org/10.1038/s41586-021-04037-6.
- Fiedler, L., and Friml, J. (2023). Rapid auxin signaling: Unknowns old and new. Curr. Opin. Plant Biol. 75, 102443. https://doi.org/10.1016/j.pbi. 2023.102443.
- Yu, Y., Tang, W., Lin, W., Li, W., Zhou, X., Li, Y., Chen, R., Zheng, R., Qin, G., Cao, W., et al. (2023). ABLs and TMKs are co-receptors for extracellular auxin. Cell 186, 5457–5471.e17. https://doi.org/10.1016/j.cell.2023. 10.017.
- Sheen, J. (2024). The new horizon of plant auxin signaling via cell-surface co-receptors. Cell Res. 34, 343–344. https://doi.org/10.1038/s41422-023-00921-0.
- Friml, J., Gallei, M., Gelová, Z., Johnson, A., Mazur, E., Monzer, A., Rodriguez, L., Roosjen, M., Verstraeten, I., Živanovič, B.D., et al. (2022). ABP1–TMK auxin perception for global phosphorylation and auxin canalization. Nature 609, 575–581. https://doi.org/10.1038/s41586-022-05187-x.
- Kuhn, A., Roosjen, M., Mutte, S., Dubey, S.M., Carrillo Carrasco, V.P., Boeren, S., Monzer, A., Koehorst, J., Kohchi, T., Nishihama, R., et al. (2024). RAF-like protein kinases mediate a deeply conserved, rapid auxin response. Cell 187, 130–148.e17. https://doi.org/10.1016/j.cell.2023. 11.021.
- Mazur, E., Kulik, I., Hajný, J., and Friml, J. (2020). Auxin canalization and vascular tissue formation by TIR1/AFB-mediated auxin signaling in

- Arabidopsis. New Phytol. 226, 1375–1383. https://doi.org/10.1111/ NPH.16446.
- Wabnik, K., Kleine-Vehn, J., Balla, J., Sauer, M., Naramoto, S., Reinöhl, V., Merks, R.M.H., Govaerts, W., and Friml, J. (2010). Emergence of tissue polarization from synergy of intracellular and extracellular auxin signaling. Mol. Syst. Biol. 6, 447. https://doi.org/10.1038/msb.2010.103.
- Abas, L., Benjamins, R., Malenica, N., Paciorek, T.T., Wiśniewska, J., Moulinier-Anzola, J.C., Sieberer, T., Friml, J., and Luschnig, C. (2006). Intracellular trafficking and proteolysis of the Arabidopsis auxin-efflux facilitator PIN2 are involved in root gravitropism. Nat. Cell Biol. 8, 249–256. https://doi.org/10.1038/ncb1369.
- Zhang, Y., Xiao, G., Wang, X., Zhang, X., and Friml, J. (2019). Evolution of fast root gravitropism in seed plants. Nat. Commun. 10, 3480. https://doi. org/10.1038/s41467-019-11471-8.
- Morita, M.T. (2010). Directional Gravity Sensing in Gravitropism. Annu. Rev. Plant Biol. 61, 705–720. https://doi.org/10.1146/annurev.arplant. 043008.092042.
- Friml, J., Wiśniewska, J., Benková, E., Mendgen, K., and Palme, K. (2002).
 Lateral relocation of auxin efflux regulator PIN3 mediates tropism in Arabidopsis. Nature 415, 806–809. https://doi.org/10.1038/415806a.
- Kleine-Vehn, J., Ding, Z., Jones, A.R., Tasaka, M., Morita, M.T., and Friml, J. (2010). Gravity-induced PIN transcytosis for polarization of auxin fluxes in gravity-sensing root cells. Proc. Natl. Acad. Sci. USA 107, 22344– 22349. https://doi.org/10.1073/pnas.1013145107.
- Luschnig, C., Gaxiola, R.A., Grisafi, P., and Fink, G.R. (1998). EIR1, a root-specific protein involved in auxin transport, is required for gravitropism in Arabidopsis thaliana. Genes Dev. 12, 2175–2187. https://doi.org/10.1101/gad.12.14.2175.
- Swarup, R., Friml, J., Marchant, A., Ljung, K., Sandberg, G., Palme, K., and Bennett, M. (2001). Localization of the auxin permease AUX1 suggests two functionally distinct hormone transport pathways operate in the Arabidopsis root apex. Genes Dev. 15, 2648–2653. https://doi.org/10.1101/gad. 210501
- Fendrych, M., Akhmanova, M., Merrin, J., Glanc, M., Hagihara, S., Takahashi, K., Uchida, N., Torii, K.U., and Friml, J. (2018). Rapid and reversible root growth inhibition by TIR1 auxin signalling. Nat. Plants 4, 453–459. https://doi.org/10.1038/s41477-018-0190-1.
- Baster, P., Robert, S., Kleine-Vehn, J., Vanneste, S., Kania, U., Grunewald, W., De Rybel, B., Beeckman, T., and Friml, J. (2013). SCFTIR1/AFB-auxin signalling regulates PIN vacuolar trafficking and auxin fluxes during root gravitropism. EMBO J. 32, 260–274. https://doi.org/10.1038/emboj. 2012.310.
- Retzer, K., Akhmanova, M., Konstantinova, N., Malínská, K., Leitner, J., Petrášek, J., and Luschnig, C. (2019). Brassinosteroid signaling delimits root gravitropism via sorting of the Arabidopsis PIN2 auxin transporter. Nat. Commun. 10, 5516. https://doi.org/10.1038/s41467-019-13543-1.
- Dubey, S.M., Han, S., Stutzman, N., Prigge, M.J., Medvecká, E., Platre, M. P., Busch, W., Fendrych, M., and Estelle, M. (2023). The AFB1 auxin receptor controls the cytoplasmic auxin response pathway in Arabidopsis thaliana. Mol. Plant 16, 1120–1130. https://doi.org/10.1016/j.molp.2023.06.008
- Tan, S., Luschnig, C., and Friml, J. (2021). Pho-view of Auxin: Reversible Protein Phosphorylation in Auxin Biosynthesis, Transport and Signaling. Mol. Plant 14, 151–165. https://doi.org/10.1016/J.MOLP.2020.11.004.
- Zourelidou, M., Absmanner, B., Weller, B., Barbosa, I.C.R., Willige, B.C., Fastner, A., Streit, V., Port, S.A., Colcombet, J., de la Fuente van Bentem, S., et al. (2014). Auxin efflux by PIN-FORMED proteins is activated by two different protein kinases, D6 PROTEIN KINASE and PINOID. eLife 3, e02860. https://doi.org/10.7554/eLife.02860.
- 34. Jia, W., Li, B., Li, S., Liang, Y., Wu, X., Ma, M., Wang, J., Gao, J., Cai, Y., Zhang, Y., et al. (2016). Mitogen-Activated Protein Kinase Cascade MKK7-MPK6 Plays Important Roles in Plant Development and Regulates Shoot





- Branching by Phosphorylating PIN1 in Arabidopsis. PLoS Biol. 14, e1002550. https://doi.org/10.1371/journal.pbio.1002550.
- Vega, A., Fredes, I., O'Brien, J., Shen, Z., Ötvös, K., Abualia, R., Benkova, E., Briggs, S.P., and Gutiérrez, R.A. (2021). Nitrate triggered phosphoproteome changes and a PIN2 phosphosite modulating root system architecture. EMBO Rep. 22, e51813. https://doi.org/10.15252/embr.202051813.
- Ötvös, K., Marconi, M., Vega, A., O'Brien, J., Johnson, A., Abualia, R., Antonielli, L., Montesinos, J.C., Zhang, Y., Tan, S., et al. (2021). Modulation of plant root growth by nitrogen source-defined regulation of polar auxin transport. EMBO J. 40, e106862. https://doi.org/10.15252/embj. 2020106862
- Kurtović, K., Vosolsobě, S., Nedvěd, D., Müller, K., Dobrev, P.I., Schmidt, V., Piszczek, P., Kuhn, A., Smoljan, A., Fisher, T.J., et al. (2025). The role of indole-3-acetic acid and characterization of PIN transporters in complex streptophyte alga Chara braunii. New Phytol. 246, 1066–1083. https:// doi.org/10.1111/nph.70019.
- Woudenberg, S., Alvarez, M.D., Rienstra, J., Levitsky, V., Mironova, V., Scarpella, E., Kuhn, A., and Weijers, D. (2024). Analysis of auxin responses in the fern Ceratopteris richardii identifies the developmental phase as a major determinant for response properties. Development 151, dev203026. https://doi.org/10.1242/dev.203026.
- Dhonukshe, P., Huang, F., Galvan-Ampudia, C.S., Mähönen, A.P., Kleine-Vehn, J., Xu, J., Quint, A., Prasad, K., Friml, J., Scheres, B., et al. (2015).
 Plasma membrane-bound AGC3 kinases phosphorylate PIN auxin carriers at TPRXS(N/S) motifs to direct apical PIN recycling. Development 142, 2386–2387. https://doi.org/10.1242/dev.127415.
- Tena, G. (2023). ABP1's new partners. Nat. Plants 9, 1941. https://doi.org/ 10.1038/s41477-023-01603-w.
- Kuhn, A., and Weijers, D. (2024). Distant cousins come to ABP1's rescue.
 Sci. China Life Sci. 67, 219–220. https://doi.org/10.1007/s11427-023-2498-0.
- Dai, N., Wang, W., Patterson, S.E., and Bleecker, A.B. (2013). The TMK Subfamily of Receptor-Like Kinases in Arabidopsis Display an Essential Role in Growth and a Reduced Sensitivity to Auxin. PLoS One 8, e60990. https://doi.org/10.1371/journal.pone.0060990.
- Gelová, Z., Gallei, M., Pernisová, M., Brunoud, G., Zhang, X., Glanc, M., Li, L., Michalko, J., Pavlovičová, Z., Verstraeten, I., et al. (2021). Developmental roles of Auxin Binding Protein 1 in Arabidopsis thaliana. Plant Sci. 303, 110750. https://doi.org/10.1016/j.plantsci.2020.110750.
- Dunwell, J.M., Purvis, A., and Khuri, S. (2004). Cupins: The most functionally diverse protein superfamily? Phytochemistry 65, 7–17. https://doi.org/10.1016/j.phytochem.2003.08.016.
- Chang, C., Schaller, G.E., Patterson, S.E., Kwok, S.F., Meyerowitz, E.M., and Bleecker, A.B. (1992). The TMKI Gene from Arabidopsis Codes for a Protein with Structural and Biochemical Characteristics of a Receptor Protein Kinase. Plant Cell 4, 1263–1271. https://doi.org/10.1105/tpc.4. 10.1263.
- Oh, M.H., Wang, X., Kota, U., Goshe, M.B., Clouse, S.D., and Huber, S.C. (2009). Tyrosine phosphorylation of the BRI1 receptor kinase emerges as a component of brassinosteroid signaling in Arabidopsis. Proc. Natl. Acad. Sci. USA 106, 658–663. https://doi.org/10.1073/PNAS.0810249106.
- Wang, X., Goshe, M.B., Soderblom, E.J., Phinney, B.S., Kuchar, J.A., Li, J., Asami, T., Yoshida, S., Huber, S.C., and Clouse, S.D. (2005). Identification and Functional Analysis of in Vivo Phosphorylation Sites of the Arabidopsis BRASSINOSTEROID-INSENSITIVE1 Receptor Kinase. Plant Cell 17, 1685–1703. https://doi.org/10.1105/TPC.105.031393.
- Xu, T., Wen, M., Nagawa, S., Fu, Y., Chen, J.G., Wu, M.J., Perrot-Rechenmann, C., Friml, J., Jones, A.M., and Yang, Z. (2010). Cell surface- and Rho GTPase-based auxin signaling controls cellular interdigitation in Arabidopsis. Cell 143, 99–110. https://doi.org/10.1016/j.cell.2010.09.003.
- Xu, T., Dai, N., Chen, J., Nagawa, S., Cao, M., Li, H., Zhou, Z., Chen, X., De Rycke, R., Rakusová, H., et al. (2014). Cell surface ABP1-TMK auxin-

- sensing complex activates ROP GTPase signaling. Science *343*, 1025–1028. https://doi.org/10.1126/science.1245125.
- Smokvarska, M., Jaillais, Y., and Martinière, A. (2021). Function of membrane domains in rho-of-plant signaling. Plant Physiol. 185, 663–681. https://doi.org/10.1093/plphys/kiaa082.
- Pan, X., Fang, L., Liu, J., Senay-Aras, B., Lin, W., Zheng, S., Zhang, T., Guo, J., Manor, U., Van Norman, J., et al. (2020). Auxin-induced signaling protein nanoclustering contributes to cell polarity formation. Nat. Commun. 11, 3914. https://doi.org/10.1038/s41467-020-17602-w.
- Kleine-Vehn, J., Leitner, J., Zwiewka, M., Sauer, M., Abas, L., Luschnig, C., and Friml, J. (2008). Differential degradation of PIN2 auxin efflux carrier by retromer-dependent vacuolar targeting. Proc. Natl. Acad. Sci. USA 105, 17812–17817. https://doi.org/10.1073/PNAS.0808073105.
- Lin, W., Zhou, X., Tang, W., Takahashi, K., Pan, X., Dai, J., Ren, H., Zhu, X., Pan, S., Zheng, H., et al. (2021). TMK-based cell-surface auxin signalling activates cell-wall acidification. Nature 599, 278–282. https://doi.org/10. 1038/s41586-021-03976-4.
- Janacek, D.P., Kolb, M., Schulz, L., Mergner, J., Kuster, B., Glanc, M., Friml, J., Ten Tusscher, K., Schwechheimer, C., and Hammes, U.Z. (2024). Transport properties of canonical PIN-FORMED proteins and the role of the loop domain in auxin transport. Dev. Cell 59, 3259–3271.e4. https://doi.org/10.1016/j.devcel.2024.09.020.
- Marquès-Bueno, M.M., Armengot, L., Noack, L.C., Bareille, J., Rodriguez, L., Platre, M.P., Bayle, V., Liu, M., Opdenacker, D., Vanneste, S., et al. (2021). Auxin-Regulated Reversible Inhibition of TMK1 Signaling by MAKR2 Modulates the Dynamics of Root Gravitropism. Curr. Biol. 31, 228–237.e10. https://doi.org/10.1016/J.CUB.2020.10.011.
- Wang, J., Chang, M., Huang, R., Gallei, M., Friml, J., Yu, Y., Wen, M., Yang, Z., and Xu, T. (2022). Self-regulation of PIN1-driven auxin transport by cell surface-based auxin signaling in Arabidopsis. Preprint at bioRxiv. https:// doi.org/10.1101/2022.11.30.518523.
- Cao, M., Chen, R., Li, P., Yu, Y., Zheng, R., Ge, D., Zheng, W., Wang, X., Gu, Y., Gelová, Z., et al. (2019). TMK1-mediated auxin signalling regulates differential growth of the apical hook. Nature 568, 240–243. https://doi. org/10.1038/s41586-019-1069-7.
- Gao, Y., Zhang, Y., Zhang, D., Dai, X., Estelle, M., and Zhao, Y. (2015).
 Auxin binding protein 1 (ABP1) is not required for either auxin signaling or Arabidopsis development. Proc. Natl. Acad. Sci. USA 112, 2275–2280. https://doi.org/10.1073/PNAS.1500365112.
- Friml, J., Vieten, A., Sauer, M., Weijers, D., Schwarz, H., Hamann, T., Offringa, R., and Jürgens, G. (2003). Efflux-dependent auxin gradients establish the apical-basal axis of Arabidopsis. Nature 426, 147–153. https://doi. org/10.1038/nature02085.
- Xu, J., and Scheres, B. (2005). Dissection of arabidopsis ADP-ribosylation factor 1 function in epidermal cell polarity. Plant Cell 17, 525–536. https:// doi.org/10.1105/tpc.104.028449.
- Asai, S., Cevik, V., Jones, J.D.G., and Shirasu, K. (2023). Cell-specific RNA profiling reveals host genes expressed in Arabidopsis cells haustoriated by downy mildew. Plant Physiol. 193, 259–270. https://doi.org/10.1093/ phys/kiad326
- Jaillais, Y., Hothorn, M., Belkhadir, Y., Dabi, T., Nimchuk, Z.L., Meyerowitz, E.M., and Chory, J. (2011). Tyrosine phosphorylation controls brassinosteroid receptor activation by triggering membrane release of its kinase inhibitor. Genes Dev. 25, 232–237. https://doi.org/10.1101/gad.2001911.
- Simon, M.L.A., Platre, M.P., Assil, S., van Wijk, R., Chen, W.Y., Chory, J., Dreux, M., Munnik, T., and Jaillais, Y. (2014). A multi-colour/multi-affinity marker set to visualize phosphoinositide dynamics in Arabidopsis. Plant J. 77, 322–337. https://doi.org/10.1111/tpj.12358.
- Karimi, M., Depicker, A., and Hilson, P. (2007). Recombinational cloning with plant gateway vectors. Plant Physiol. 145, 1144–1154. https://doi. org/10.1104/pp.107.106989.
- Lampropoulos, A., Sutikovic, Z., Wenzl, C., Maegele, I., Lohmann, J.U., and Forner, J. (2013). GreenGate - A novel, versatile, and efficient cloning





- system for plant transgenesis. PLOS One 8, e83043. https://doi.org/10.1371/journal.pone.0083043.
- Huang, R., Zheng, R., He, J., Zhou, Z., Wang, J., Xiong, Y., and Xu, T. (2019). Noncanonical auxin signaling regulates cell division pattern during lateral root development. Proc. Natl. Acad. Sci. USA *116*, 21285–21290. https://doi.org/10.1073/pnas.1910916116.
- Ashkenazy, H., Abadi, S., Martz, E., Chay, O., Mayrose, I., Pupko, T., and Ben-Tal, N. (2016). ConSurf 2016: an improved methodology to estimate and visualize evolutionary conservation in macromolecules. Nucleic Acids Res. 44, W344–W350. https://doi.org/10.1093/NAR/GKW408.
- Yariv, B., Yariv, E., Kessel, A., Masrati, G., Chorin, A.B., Martz, E., Mayrose, I., Pupko, T., and Ben-Tal, N. (2023). Using evolutionary data to make sense of macromolecules with a "face-lifted" ConSurf. Protein Sci. 32, e4582. https://doi.org/10.1002/pro.4582.
- Jumper, J., Evans, R., Pritzel, A., Green, T., Figurnov, M., Ronneberger, O., Tunyasuvunakool, K., Bates, R., Žídek, A., Potapenko, A., et al. (2021). Highly accurate protein structure prediction with AlphaFold. Nature 596, 583–589. https://doi.org/10.1038/s41586-021-03819-2.
- Madeira, F., Pearce, M., Tivey, A.R.N., Basutkar, P., Lee, J., Edbali, O., Madhusoodanan, N., Kolesnikov, A., and Lopez, R. (2022). Search and sequence analysis tools services from EMBL-EBI in 2022. Nucleic Acids Res. 50, W276–W279. https://doi.org/10.1093/NAR/GKAC240.
- Waterhouse, A.M., Procter, J.B., Martin, D.M.A., Clamp, M., and Barton, G.J. (2009). Jalview Version 2—A multiple sequence alignment editor and analysis workbench. Bioinformatics 25, 1189–1191. https://doi.org/ 10.1093/BIOINFORMATICS/BTP033.
- Reiser, L., Subramaniam, S., Zhang, P., and Berardini, T. (2022). Using the Arabidopsis Information Resource (TAIR) to Find Information About Arabidopsis Genes. Curr. Protoc. 2, e574. https://doi.org/10.1002/cpz1.574.
- Mi, H., Muruganujan, A., Casagrande, J.T., and Thomas, P.D. (2013).
 Large-scale gene function analysis with the panther classification system.
 Nat. Protoc. 8, 1551–1566. https://doi.org/10.1038/nprot.2013.092.
- Supek, F., Bošnjak, M., Škunca, N., and Šmuc, T. (2011). REVIGO Summarizes and Visualizes Long Lists of Gene Ontology Terms. PLoS One 6, e21800. https://doi.org/10.1371/journal.pone.0021800.
- 75. Zhang, H., Zhang, F., Yu, Y., Feng, L., Jia, J., Liu, B., Li, B., Guo, H., and Zhai, J. (2020). A Comprehensive Online Database for Exploring

- $\sim\!\!20,\!000$ Public Arabidopsis RNA-Seq Libraries. Mol. Plant 13, 1231–1233. https://doi.org/10.1016/j.molp.2020.08.001.
- Czechowski, T., Stitt, M., Altmann, T., Udvardi, M.K., and Scheible, W.R. (2005). Genome-wide identification and testing of superior reference genes for transcript normalization in arabidopsis. Plant Physiol. 139, 5–17. https://doi.org/10.1104/pp.105.063743.
- 77. Grones, P., Chen, X., Simon, S., Kaufmann, W.A., De Rycke, R., Nodzyński, T., Zažímalová, E., and Friml, J. (2015). Auxin-binding pocket of ABP1 is crucial for its gain-of-function cellular and developmental roles. J. Exp. Bot. 66, 5055–5065. https://doi.org/10.1093/jxb/erv177.
- Malamy, J.E., and Benfey, P.N. (1997). Organization and cell differentiation in lateral roots of Arabidopsis thaliana. Development 124, 33–44. https://doi.org/10.1242/dev.124.1.33.
- Xu, W., Ding, G., Yokawa, K., Baluška, F., Li, Q.F., Liu, Y., Shi, W., Liang, J., and Zhang, J. (2013). An improved agar-plate method for studying root growth and response of Arabidopsis thaliana. Sci. Rep. 3, 1273. https:// doi.org/10.1038/srep01273.
- Thomas, M., Soriano, A., O'Connor, C., Crabos, A., Nacry, P., Thompson, M., Hrabak, E., Divol, F., and Péret, B. (2023). Pin2 Mutant Agravitropic Root Phenotype Is Conditional and Nutrient-Sensitive. Plant Sci. 329, 111606. https://doi.org/10.1016/j.plantsci.2023.111606.
- von Wangenheim, D., Hauschild, R., Fendrych, M., Barone, V., Benková, E., and Friml, J. (2017). Live tracking of moving samples in confocal microscopy for vertically grown roots. eLife 6, e26792. https://doi.org/10.7554/eLife.26792.
- Hayashi, Y., Nakamura, S., Takemiya, A., Takahashi, Y., Shimazaki, K.I., and Kinoshita, T. (2010). Biochemical Characterization of In Vitro Phosphorylation and Dephosphorylation of the Plasma Membrane H+-ATPase. Plant Cell Physiol. 51, 1186–1196. https://doi.org/10.1093/pcp/pcq078.
- Tan, S., Abas, M., Verstraeten, I., Glanc, M., Molnár, G., Hajný, J., Lasák, P., Petřík, I., Russinova, E., Petrášek, J., et al. (2020). Salicylic Acid Targets Protein Phosphatase 2A to Attenuate Growth in Plants. Curr. Biol. 30, 381–395.e8. https://doi.org/10.1016/j.cub.2019.11.058.
- Brady, S.M., Orlando, D.A., Lee, J.Y., Wang, J.Y., Koch, J., Dinneny, J.R., Mace, D., Ohler, U., and Benfey, P.N. (2007). A high-resolution root spatiotemporal map reveals dominant expression patterns. Science 318, 801–806. https://doi.org/10.1126/SCIENCE.1146265.





STAR*METHODS

KEY RESOURCES TABLE

REAGENT or RESOURCE	SOURCE	IDENTIFIER
Antibodies		
Anti-mCherry, rabbit	Abcam	Cat# ab167453; RRID:AB_2571870
Anti-HA-Peroxidase	Sigma Aldrich	Cat# 12013819001; RRID:AB_390917
Anti-FLAG®M2-Peroxidase (HRP)	Sigma Aldrich	Cat# A8592; RRID:AB_439702
Anti-ROP2, rabbit	Abiocode	Cat# R2165-2
Anti-ROP6, rabbit	Abiocode	Cat# R2142-1
Anti-TMK1, rabbit	Cao et al. ⁵⁷	N/A
Anti-TMK1, rabbit	Biosite/THP Medical	Cat #ASJ-FADMZZ-100
Anti-AHA2, rabbit	Hayashi et al.82	N/A
PhosTag Biotin Probe	FUJIFILM Wako	Cat# BTL-111
Anti-PIN2	Abas et al. ²¹	N/A
Goat Anti-rabbit-HRP	Agrisera	Cat# AS09 602; RRID:AB_1966902
Bacterial and virus strains		
Escherichia coli DH5a	In-house	N/A
Escherichia coli BL21	In-house	N/A
Escherichia coli BL21 (DE3)	In-house	N/A
Agrobacterium tumefaciens GV3101	In-house	N/A
Chemicals, peptides, and recombinant proteins		
6HIS-PIN2-HL	Tan et al. ⁸³	N/A
AA	Duchefa	Cat# 10901
DMSO	Thermo Fisher Scientific	Cat# 022914.K2
NPA	Duchefa	Cat# N0926
Friton X-100	Sigma Aldrich	Cat# 1.08603
cOmplete, EDTA-free Protease	Roche	Cat# 4693132001
nhibitor Cocktail		
Phosophatase Inhibitor Cocktail	Roche	Cat# 4906837001
Nonidet P-40	Sigma Aldrich	Cat# 74385
PTG	Thermo Fisher Scientific	Cat# R0392
PMSF	Sigma Aldrich	Cat# 78830
Tween 20	Sigma Aldrich	Cat# P9416
TTC	Sigma Aldrich	Cat# D0632
Quick Start™ Bradford Reagent	Bio-Rad	Cat# 5000201
ГСЕР	Sigma Aldrich	Cat# C4706
Na3VO4	Sigma Aldrich	Cat# 450243
midazole	Sigma Aldrich	Cat# I5513
Bio-Safe™ Coomassie Stain	Bio-Rad	Cat# 1610786
Dexamethasone	Sigma Aldrich	Cat# D1756
γ-32P]-ATP	Perkin-Elmer	Cat #NEG502A001MC
RNeasy Plant Mini Kit	Qiagen	Cat# 74904
QuantiNova Reverse Transcription Kit	Qiagen	Cat# 205411
Luna® Universal qPCR mastermix	NEB	Cat# M3003
4-15% Mini-PROTEAN®TGX™ Precast Protein Gels	Bio-Rad	Cat# 4561084
SuperSignal West Femto Maximum Sensitivity Substrate detection kit	Thermo Fisher Scientific	Cat# 34094

(Continued on next page)





Continued		
REAGENT or RESOURCE	SOURCE	IDENTIFIER
μMACS Epitope Tag Protein Isolation Kit	Miltenyi Biotec	Cat# 130-091-122
Glycine	Bio-Rad	Cat# 1610724
ChromoTek RFP-Trap Magnetic Agarose	Proteintech	Cat #rtma-20
HisPurTM Ni-NTA Magnetic Beads	Thermo Fisher Scientific	Cat# A50591
SDS loading dye (4X Laemmli Sample Buffer)	Bio-Rad	Cat# 1610747
Ni-NTA His affinity agarose	Thermo Fisher Scientific	Cat# R90110
Anti-HA Affinity Matrix	Sigma Aldrich	Cat# 11815016001
Experimental models: Organisms/strains		
Col-0	Widely distributed	N/A
abp1-C1	Friml et al. 17	N/A
abp1-TD1	Friml et al. 17	N/A
abl3-1	This paper	N/A
abl3-2	This paper	N/A
abp1-C1;abl3-1	This paper	N/A
abp1-TD1;abl3-1	This paper	N/A
abp1-TD1;abl3-2	This paper	N/A
tmk1-1	Cao et al. ⁵⁷	N/A
TMK1::qTMK1-GFP;tmk1-1	This paper	N/A
TMK1::gTMK1-FLAG;tmk1-1	Cao et al. ⁵⁷	N/A
TMK1::GUS	Friml et al. ¹⁷	N/A
TMK2::GUS	Friml et al. 17	N/A
TMK3::GUS	Friml et al. 17	N/A
TMK4::GUS	Friml et al. 17	N/A
ABL3::GUS	Asai et al. ⁶¹	N/A
35S::ABL3-6xHIS-3xFLAG (35S::ABL3-HF)	Asai et al. ⁶¹	N/A
eir1-4	Abas et al. ²¹	N/A
PIN2::PIN2 ^{WT} -GFP;eir-1-4	This paper	N/A
PIN2::PIN2 ^{5-MIMIC} -GFP;eir-1-4	This paper	N/A
PIN2::PIN2 ^{5-DEAD} -GFP;eir-1-4	This paper	N/A
CRAP;WT	This paper	N/A
CRAP;tmk1-1	This paper	N/A
CRAP ^{T20N} ;WT (GDP-LOCKED)	This paper	N/A
PIN2::PIN2-GFP;WT	Xu and Scheres ⁶⁰	N/A
PIN2::PIN2-GFP;tmk1-1	This paper	N/A
PIN2::PIN2-GFP;abp1-TD1;abl3-1	This paper	N/A
DR5rev::GFP;WT	Friml et al. ⁵⁹	N/A
DR5rev::GFP;tmk1-1	This paper	N/A
UBQ10::TMK1 ^{K616R} -2XmCherry	This paper	N/A
UBQ10::TMK1 ^{K616R} -2XmCherry X PIN2::PIN2-GFP;WT [F1 generation]	This paper	N/A
TMK1::gTMK1-GFP;tmk1-1 X PIN2::PIN2-mCherry;WT [F1 generation]	This paper	N/A
UBQ10::gTMK1-3xHA	This paper	N/A
DEX::TMK1 ^{K616R} -HA	Li et al. ¹³	N/A
Oligonucleotides		
Primers are listed in Table S1	This paper	N/A
Recombinant DNA		
pB7m24GW.3, PIN2::PIN2 ^{WT} -EGFP	This paper	N/A
pB7m24GW.3, PIN2::PIN2 ^{5-MIMIC} -EGFP	This paper	N/A

(Continued on next page)





Continued		
REAGENT or RESOURCE	SOURCE	IDENTIFIER
pB7m24GW.3, PIN2::PIN2 ^{5-DEAD} -EGFP	This paper	N/A
pB7WG2, 35S::ABL3-HA	This paper	N/A
pB7WG2, 35S::ABL3-mCherry	This paper	N/A
pB7WG2, 35S::TMK1-HA	This paper	N/A
pB7WG2, 35S::TMK1-mCherry	This paper	N/A
pB7WG2, 35S::FLS2-GFP	This paper	N/A
pB7WG2, 35S::PIN2-mCherry	This paper	N/A
pB7m34GW, TMK1::gTMK1-GFP	This paper	N/A
pB7m34GW, 35S::gTMK1 ^{ΔKD} -GFP	This paper	N/A
CRAP	This paper	N/A
CRAP ^{T20N} (GDP-LOCKED)	This paper	N/A
pH7m34GW, UBQ10::TMK1 ^{K616R} -2xmCherry	This paper	N/A
pDEST-His-MBP-CRIB	This paper	N/A
Software and algorithms		
R version 4.0.4	R Core Team	R: The R Project for Statistical Computing
REVIGO version 1.8.1	Supek et al.74	http://revigo.irb.hr/
AlphaFold2 version 2.2.4	Jumper et al. ⁶⁹	https://github.com/google-deepmind/alphafold
Consurf	Yariv et al. ⁶⁸	https://consurf.tau.ac.il/
AuxPhos	Kuhn et al. ¹⁸	https://weijerslab.shinyapps.io/AuxPhos/
MUSCLE version 3.8.425	Madeira et al. ⁷⁰	https://www.ebi.ac.uk/jdispatcher/msa/muscle?stype=protein
Jalview version 2.11.4.1	Waterhouse et al.71	https://www.jalview.org/
ImageJ	NIH	https://imagej.nih.gov/ij/

EXPERIMENTAL MODEL AND STUDY PARTICIPANT DETAILS

Molecular cloning, plant material, and growth conditions

All mutant alleles were in the *Columbia-0* (*Col-0*) background except *abp1-TD1*, which was in *Columbia-4* (*Col-4*). The T-DNA insertion lines *eir1-4* (SALK_091142) and *tmk1-1* (SALK_016360) were previously reported, ^{21,57} as was *abp1-C1* (CRISPR) and *abp1-TD1*⁵⁸ (SK21825). The T-DNA insertion line SAIL_441_G04, which harbors four insertions, was obtained from NASC and crossed with Col-0. Insertion-specific primers (Table S1) were then used to out-segregate the SAILSEQ_441_G04.2 insertion in *ABL3/AT4G14630* from SAILSEQ_441_G04.0 (AT4G09510), SAILSEQ_441_G04.1 (AT4G02930), and SAILSEQ_441_G04.3 (AT5G09590), yielding *abl3-1*. To obtain *abp1-C1;abl13-1* and *abp1-TD1;abl3-1*, we crossed the respective *abp1* mutants with *abl3-1*. The T-DNA insertion line SALK_203089C was obtained from NASC, verified by genotyping (Table S1), and used as *abl3-2*. The *abp1-TD1;abl3-2* double mutant was obtained by genetic crosses.

PIN2::PIN2-GFP, DR5rev::GFP, TMK1::TMK1-FLAG;tmk1-1, TMK1::GUS, TMK2::GUS, TMK3::GUS, and TMK4::GUS were described before. ^{17,57,59,60} We generated PIN2::PIN2-GFP;tmk1-1 and DR5rev::GFP;tmk1-1 by genetic crosses of the respective markers with tmk1-1. We generated PIN2::PIN2-GFP;abp1-TD1;abl3-1 by a genetic cross with abp1-TD1;abl3-1. Shuta Asai kindly provided the ABL3::GUS and 35S::ABL3-6xHIS-3xFLAG lines. ⁶¹ DEX::TMK1^{K616R}-HA line was published before. ¹³ To generate TMK1::TMK1-GFP and 35S::TMK1^{ΔKD}-GFP, the TMK1 full length or TMK1^{ΔKD} (amino acid 1-587) genomic DNA without a stop codon were amplified from CoI-0 DNA through PCR with TMK1-FL-B1-F and TMK1-FL-B2-R/TMK1-ΔKD-B2-R primers (Table S1), respectively. The resulting TMK1 sequences were inserted into pDONR221 by a BP reaction. Next, for the TMK1::TMK1-GFP construct, pDONR P4-P1R pTMK1, pDONR221 gTMK1, and pDONR P2R-P3 GFP; for 35S::TMK1^{ΔKD}-GFP, pDONR P4-P1R p35S, pDONR221 gTMK1^{ΔKD} and pDONR P2R-P3 GFP were recombined into pB7m34GW vector by a MultiSite Gateway LR reaction. To generate UBQ10::TMK1^{K616R}-2xmCherry, TMK1^{K616R}noSTOP/pDONR221 was obtained by site-directed mutagenesis, amplifying pDONR221 TMK1 with the TMK1KD-K616F and TMK1KD-K616R primer pair. pDONR221-TMK1^{K616R} was then recombined by LR reaction with pDONR P4-P1R pUBQ10, ⁶² pDONR P2R-P3 2xmCHERRY-4xMyc⁶³ and pH7m34GW to obtain UBQ10:: TMK1^{K616R}-2xmCherry in pH7m34GW.

To clone PIN2 phospho-lines, Gibson Assembly (NEBuilder® HiFi DNA Assembly Master Mix, E2621L) was used to insert EGFP into the PIN2 coding sequence between Thr405 and Arg406 (according to Vega et al. 35) and to assemble this fragment with an attL sitescontaining pDONR221 backbone (Table S1), yielding pDONR221 PIN2WT-EGFP. For 5-MIMIC and 5-DEAD constructs, we used gene synthesis (Integrated DNA Technologies, IDT) to obtain 1533-bp blocks containing EGFP and its flanking PIN2 CDS sequences with





Ser179, Ser183, Thr233, Ser393, Ser439 triplets mutated to either GAC (Asp, 5-MIMIC) or GCC (Ala, 5-DEAD) (Table S1). These were Gibson-Assembled with a backbone fragment amplified from the *pDONR221 PIN2*^{WT}-EGFP plasmid (Table S1), yielding *pDONR221 PIN2*^{5-MIMIC}-EGFP and *pDONR221 PIN2*^{5-DEAD}-EGFP. Finally, the pDONR221 plasmids were recombined with pDONR-P4-P1R-pPIN2²² into pB7m24GW.3 by a multisite LR reaction (Gateway), and *eir1-4* (*pin2* null)²¹ was used for dipping.

The CRAP sensor was cloned using a combination of Gibson Assembly and the GreenGate approach. First, each GreenGate block was generated by fusing two PCR fragments – vector backbone and the respective CDS. ROP2 promoter fragment was subcloned into pGGA backbone fragment digested by Bsal. To obtain a non-ratiometric CRAP sensor, the following fragments were fused: pGGA-ROP2p. + pGGB-CRIB + pGGC-cpGFP + pGGD-ROP2 + pGGE009(UBI10term.) + pGGF-HYG. The resulting destination vector was sequenced and used as a template for cloning the entire CRAP CDS into a pGGD vector. This vector was then used in the GreenGate reaction to add the mCHERRY ratiometric control: pGGA-ROP2p + pGGB-mCHERRY-ROP2_UBI10term. + pGGC015 (mCHERRY)-pGGD-CRAP-pGGE-HSP18.2term + pGGF005(HYG). ROP2-UBI10 fragment was amplified from the non-ratiometric CRAP sensor. Point mutagenesis to generate the dominant negative T20N mutation into ROP2 was performed as a single fragment Gibson Assembly with point-mutated compatible cohesive ends. The common building blocks were obtained from 65 (pGGC015, pGGE-009, pGGF005). The pGGZ001 block with exchanged bacterial selection cassette (kanamycin) and pGGE-HSP18term was kindly provided by Dr. Andrea Bleckmann. The CRAP sensor was dipped into Col-0 to obtain *CRAP;WT* and this line was subsequently crossed with *tmk1-1* to obtain *CRAP;tmk1-1*.

To obtain seedlings co-expressing TMK1-GFP and PIN2-mCherry, we crossed *TMK1::TMK1-GFP;tmk1-1*⁶⁶ with *PIN2::PIN2-mCherry;eir-1-4* (kind gift by Christian Luschnig) and imaged the F1 generation.

To obtain a plasmid for protein expression of His-MBP-CRIB, pDEST-His-MBP (Thermo Fisher Scientific) was used for backbone amplification with HIS_MBP_REV and HIS_MBP_FOR primers (Table S1). Then, CRIB domain was cloned from Arabidopsis cDNA with CRIB_REV and CRIB_FOR primers (Table S1). The resultant amplicons were Gibson Assembled together (see above).

All constructs were transformed into the *Agrobacterium tumefaciens* strain pGV3101 by electroporation and further into plants by the floral dip method. The T2 generation was screened for single insertions, and homozygous T3 lines were used for experiments. Arabidopsis seeds were surface-sterilized with 70% (v/v) ethanol for 20 min, followed by commercial bleach (2.5% [v/v] sodium hypochlorite) containing 0.05% (v/v) Triton X-100 for 10 min, and finally washed four times with sterile water. Seed stratification was conducted in the dark at 4°C for 2 days. Unless indicated otherwise, seedlings were grown at 22°C on ½ MS plates with 1% agar and 1% sucrose, or in soil with 16h light/8h dark cycles, photoperiod at 80 to 100 mE m⁻² sec⁻¹.

METHOD DETAILS

Bioinformatics

Phospho-proteomic analyses used data from Friml et al., ¹⁷ Kuhn et al., ¹⁸ and Woudenberg et al. ³⁸ Time-course profiles of auxin-induced phosphorylation were obtained with the AuxPhos tool (https://weijerslab.shinyapps.io/AuxPhos). ¹⁸ Evolutionary rates for PIN1, PIN2, and PIN3 amino acids were calculated as ConSurt^{67,68} conservation scores and projected on the respective AlphaFold⁶⁹ structures for visualization. Multiple sequence alignment of PIN2 orthologs (Uniprot IDs: Q9LU77, F6GXI9, E5KGD3, A0A251QTL1, A0A1D6P5D8, Q651V6, W1PK04, B5TXD0) or ABP1/ABLs (Uniprot IDs: P33487, P13689, P94040, P94072, Q9LEA7) was done with the MUSCLE tool available from EMBL-EBI⁷⁰ and visualized in Jalview. ⁷¹

For gene ontology enrichment, the "mock ABP1-TMK1 phospho-proteome" comprised Ensembl protein IDs of proteins concurrently hypo-phosphorylated in both *abp1-TD1* and *tmk1-1* mutants under mock conditions or—in the case of the "auxin-treated ABP1-TMK1 phospho-proteome"—auxin (2 min, 100 nM IAA) conditions.¹⁷ These were submitted to the PANTHER extension of the TAIR database^{72,73} and queried for molecular function with all *Arabidopsis thaliana* proteins as a reference list. Annotation version and release date: [GO Ontology database https://doi.org/10.5281/zenodo.12173881 Released 2024-06-17]. Enrichment calculation was using Fisher's Exact Test with a Bonferroni correction (p<0.05). The resultant terms were processed in REVIGO⁷⁴ (parameters: medium list size of 0.7, clustering variables: p-value or fold enrichment, removal of obsolete GO terms, whole Uniprot reference set, SimRel semantic similarity) and visualized as treemaps with arbitrary coloring.

Plant pictograms were obtained from the Bioicons project under the MIT license. Attributions: Arabidopsis_thaliana icon by DBCLS https://togotv.dbcls.jp/en/pics.html is licensed under CC-BY 4.0 Unported https://creativecommons.org/licenses/by/4.0/. Zea_mays_cartoon icon by Daniel Carvalho https://figshare.com/authors/Plant_Illustrations/3773596 is licensed under CC-BY 4.0 Unported https://creativecommons.org/licenses/by/4.0/. DicotSeedling icon https://github.com/ginavong by Gina-Vong is licensed under CC0 https://creativecommons.org/publicdomain/zero/1.0/. The conifer branch pictogram was obtained from the free-for-use Pixabay repository.

The crystal structure of maize ABP1 (PDB ID: 1LRH) was superimposed with the AlphaFold2 structure of ABL3 (Uniprot ID: Q9LEA7) with the "super" command in Pymol. Tissue-specific expression profiles for ABL1, ABL2, ABP1, ABL3, TMK1, TMK2, TMK3 and TMK4 were compiled using a database of \sim 20,000 public Arabidopsis RNAseq experiments.

RT-qPCR

Total RNA was prepared from max. 100 mg of roots of 4-day-old seedlings according to the RNeasy Plant Mini Kit (Qiagen). cDNA was synthesized from 1µg of total mRNA using the QuantiNova Reverse Transcription Kit (Qiagen). Mutant expression analyses used





3-4 biological and 3 technical replicates pipetted into a 384-well plate using an automated JANUS Workstation (PerkinElmer). According to the manufacturer's instructions, 5 μ L reaction volume contained 2.5 μ L Luna® Universal qPCR mastermix (NEB). RT-qPCR analyses were performed using the Real-time PCR Roche Lightcycler 480 and control PP2AA3 (At1G13320) primers were used as in Czechowski et al. ⁷⁶ For each of the evaluated genes, three different primer pairs were tested (Table S1); except the *PIN2-GFP* phospho-line transgene, which was quantified using a single pair of primers without testing multiple sets.

Fluorescence lifetime imaging

FRET-FLIM experiments were performed in protoplasts isolated from Arabidopsis root cell suspension as described previously. 77 10 μ g of plasmid DNA (TMK1-GFP, TMK1 $^{\Delta KD}$ -GFP, PIN2-mCherry, FLS2-GFP) were used for protoplast transfection, followed by incubation in a sterile 24-well microtiter plate overnight in the dark at room temperature. FRET-FLIM experiments were performed using a TriM Scope II inverted 2-photon microscope equipped with a FLIM X16 TCSPC Detector for time-correlated single photon counting (LaVision BioTec). Fluorescence lifetime image stacks (150 slices, with 0,082 ns time interval) were acquired. Image analyses were done in Fiji by performing a threshold mask from the sum projection of each stack and by averaging all the pixels at each time point of the stack. To yield an exponential decay with offset, the intensity at time point 0 was normalized.

GUS staining

4-day-old seedlings were stained in 0.1 M sodium phosphate buffer (pH 7.0) containing 0.1% X-GlcA sodium salt, 1 mM K_3 [Fe(CN)₆], 1 mM K_4 [Fe(CN)₆] and 0.05% Triton X-100 for 20 min (*TMK1::GUS*), 2 h (*TMK4::GUS*, *TMK2::GUS*, *ABL3::GUS*) or 6 h (*TMK3::GUS*) at 37°C. Further, samples were incubated overnight in 80% (v/v) ethanol at room temperature. Tissue clearing was conducted as previously described. BIC microscopy for analysis of the GUS staining assay was performed using an Olympus BX53 microscope equipped with 10x and 20x air objectives and a DP26 CCD camera.

Root gravitropic assays

For sensitive phenotyping of the gravitropic response, unless indicated otherwise, seeds were germinated on sucrose-free ½ MS plates with 1% agar. ^{26,79,80} 5-day-old seedlings were transferred to a fresh plate and incubated in a vertical position for 40 minutes to recover. For contrast, a square of moist black paper was placed inside the lid of the plate. After rotation by 90°, the roots were imaged every 30 min on a vertical flatbed scanner (Epson Perfection V370 Photo). Image time series were stabilized using the StackReg Fiji plugin. Root curvature was analyzed with the Manual Tracking Fiji plugin and angles were calculated from root tip positions over time in Microsoft Excel.

Imaging of transgenic lines

Confocal microscopy was performed on a vertical Zeiss LSM800 microscope⁸¹ equipped with a 20X Plan Apochromat air objective (NA = 0.8). GFP- and mCherry-tagged proteins [PIN2-GFP, TMK1-GFP, CRAP (mCherry/GFP), DR5rev::GFP] were excited at 488 and 561 nm, respectively, with emission collected in the following ranges: 490-576 nm or 560-700 nm, respectively.

PIN2-GFP phospho-lines were imaged by taking 12 Z-sections spanning the whole volume of each root. These were processed through "maximum intensity" projection in Fiji and total GFP signal was quantified across epidermal and cortical regions.

For imaging of *PIN2::PIN2-GFP* and *DR5rev::GFP* asymmetric distribution, 5-day-old seedlings were placed in a 1-well chambered coverglass (VWR, Kammerdeckglaser, Lab-Tek, Nunc, catalog number 734-2056) with a block of solid ½ MS medium, ⁸¹ optionally supplemented with mock or 10 µM NPA according to the experiment. For recovery, the chamber was incubated vertically in darkness for 2 h before imaging. Ten Z-sections spaced 1 µm for *PIN2::PIN2-GFP* and 4.5 µm for *DR5rev::GFP* were collected in the median root section before and after 90° rotation at the indicated time points. The "sum slices" intensity projection in Fiji was then applied. Marking epidermal and cortical regions together, the mean grey value was quantified as per.²⁹

The CRAP sensor was validated by auxin treatments in a microfluidic vRootchip setup described previously. ^{13,28} For CRAP sensor imaging during gravistimulation, 5-day-old seedlings were placed vertically in a 1-well chambered coverglass with a block of solid 1/2 MS agar. The chamber was fitted inside a rotational stage. Seedlings were gravistimulated by turning the stage by 90°, achieving horizontal root position, and subsequently flipping the stage by 180°. Each root was imaged every 8.94 s for 15 min three times (with 180° flips in between) as technical replicates. GFP and mCherry signals were recorded simultaneously as a single track. Mean grey values at the lower and upper root sides were quantified. Next, the 561/488 nm ratio indicative of ROP activity was calculated for the upper and lower root sides. Finally, to compare ROP activity between the two sides, the lower root side ratio was divided by the upper root side ratio and plotted over time, averaging the three technical replicates for each single root. For visual representation, a root with a strong CRAP asymmetry was used. The last 10 time points of the 15-min imaging time course were averaged, and the pixel ratios reflecting CRAP activation were calculated as [mCherry - mCherry background] / [GFP - GFP background]. For plotting, the alpha value was derived from intensity and the Gaussian difference of the mCherry reference channel to suppress artifacts from numeric instability in low-intensity regions.

Microsomal protein extraction

4-day-old-seedling roots were harvested, ground to powder in liquid nitrogen, and vortexed vigorously in extraction buffer 1 [50 mM Tris-HCl pH 7.5, 150 mM NaCl, Complete EDTA-free Protease Inhibitor cocktail (Roche), PhosSTOP phosphatase inhibitor cocktail





(Roche)] in 1/10 (w/v) ratio. The resulting homogenate was centrifuged at 20000 g for 30 min at 4°C. The pellet was resuspended in extraction buffer 2 [50 mM Tris–HCl pH 7.5, 150 mM NaCl, 0.5% Nonidet P-40, 1% Triton X-100, Complete EDTA-free Protease Inhibitor cocktail (Roche), PhosSTOP phosphatase inhibitor cocktail (Roche)], and centrifuged at 12000 g for 20 min at 4°C. Bradford assay was used to quantify protein in the supernatant. Samples were separated by SDS-PAGE (4-15% Mini-PROTEAN®TGXTM Precast Protein Gels (Bio-Rad)), transferred to a PVDF (polyvinylidene difluoride) membrane, and immuno-blotted using the following primary antibodies: affinity-purified TMK1 (1:1000), ⁵⁷ AHA2 (1:1000), ⁸² PIN2 (1:1000)²¹ antibodies and anti-ROP6 (1:1000, Abiocode). The secondary antibody was anti-Rabbit-HRP (1:5000, Agrisera, AS09 602). Detection was done using the SuperSignal West Femto Maximum Sensitivity Substrate detection kit (ThermoFisher Scientific) and the Amersham 600RGB imager (GE Healthcare).

CETSA

For CETSA from protoplasts, $10 \,\mu g$ of plasmid DNA (35S::gGLP9-HA) was used for protoplast transfection, followed by incubation in a sterile 24-well microtiter plate overnight in the dark at room temperature. The incubation buffer was exchanged for protein extraction buffer ($50 \,m M$ Tris-HCl, pH 7.6, $150 \,m M$ NaCl, $10 \,\%$ glycerol, $5 \,m M$ DTT, $1 \,m M$ PMSF, $0.5 \,\%$ NP-40, complete Roche protease inhibitors) and protoplasts were lysed by $10 \,v igorous$ ice-vortexing(5s)-ice cycles, $30 \,m in$ rotation at $4 \,^{\circ}C$, and again $10 \,v igorous$ ice-vortexing(5s)-ice cycles. The lysate was centrifuged twice at maximum speed for $10 \,m inutes$ ($4 \,^{\circ}C$) in a table-top centrifuge. The final supernatant represented the protein extract, which was first sampled for Western blotting and then split into two halves supplemented with either $100 \,\mu M$ IAA or mock treatment. IAA- or mock-treated extracts were incubated for $1 \,h$ on ice with occasional mixing. Next, the extracts were aliquoted for a $3 \,m in$ incubation at temperatures between $42 \,m d$ $4 \,^{\circ}C$ in a PCR machine (Bio-Rad) and returned to ice immediately. Finally, the samples were spun down in a tabletop centrifuge ($12,000 \,m m$, $6 \,m in$, $4 \,^{\circ}C$) and the supernatants were carefully transferred to new tubes for Western blotting (Anti-HA-HRP as described above).

CETSA from 5-day-old 35S::ABL3-6xHIS-3xFLAG Arabidopsis seedlings used the same buffer and protocol with the only difference being the protein extraction procedure and the use of a different antibody for Western blotting (anti-FLAG®M2-Peroxidase (HRP), Sigma). Protein was extracted by adding ice-cold buffer to liquid-nitrogen-ground tissue, followed by centrifugation and supernatant collection as described for protoplast proteins.

Western blot analysis of phosphorylated proteins

To analyze the phosphorylation status of TMK1 *in planta*, after corresponding treatment, 4-day-old *tmk1-1* roots expressing *TMK1:: TMK1-FLAG* were ground to powder in liquid nitrogen and homogenized in ice-cold sucrose buffer [20 mM Tris–HCl pH 8, 0.33 M sucrose, Complete EDTA-free Protease Inhibitor cocktail (Roche), PhosSTOP phosphatase inhibitor cocktail (Roche)], followed by a centrifugation step at 5000 g for 10 min at 4°C. To obtain the membrane protein fraction, the supernatant was centrifuged at 20000 g for 30 min at 4°C and the resulting pellet was solubilized with lysis buffer [20 mM Tris–HCl pH 8, 150 mM NaCl, 1% TritonX100, Complete EDTA-free Protease Inhibitor cocktail (Roche), PhosSTOP phosphatase inhibitor cocktail (Roche)] and centrifuged at 20000 g for 10 min at 4°C. The corresponding supernatant was used for immunoprecipitation assay with anti-FLAG microbeads according to the manufacturer's instructions (μMACS Epitope Tag Protein Isolation Kit (MACS Miltenyi Biotec)). Samples were separated by SDS-PAGE (4-15% Mini-PROTEAN®TGXTM Precast Protein Gels (Bio-RAD)) and transferred to a PVDF membrane, which was blotted with anti-FLAG®M2-Peroxidase (HRP) (Sigma) to detect total immunoprecipitated protein. Next, the membrane was stripped in 7 mL of mild stripping buffer (Abcam, 1 L: 15 g glycine, 1 g SDS, 10 mL Tween-20, pH 2.2) for 5 min, and the incubation was repeated with fresh buffer. The membrane was washed (2x 10 min in PBS, 2x 5 min in TBST) and re-blocked. The Phos-tag BTL-111 probe was then used according to the manufacturer's instructions (www.wako-chem.co.jp) to detect phosphorylated protein levels

Co-immunoprecipitation assays

4-day-old *tmk1-1* seedlings expressing TMK1::TMK1-FLAG were treated with 5, 20 nM IAA or DMSO control for 30 minutes. Roots were harvested, ground to powder in liquid nitrogen, and subjected to protein microsomal fraction extraction. Solubilized proteins from microsomal fraction were immunoprecipitated using super-paramagnetic μMACS beads coupled to monoclonal anti-FLAG antibody according to the manufacturer's instructions (Miltenyi Biotec). WT Col-0 extract was used as a control of the unspecific binding of endogenous PIN2. Proteins immunoprecipitated with anti-FLAG antibody were separated by SDS-PAGE (4-15% Mini-PROTEAN®TGXTM Precast Protein Gels (Bio-RAD)), transferred to a PVDF membrane and analyzed by immunoblot with anti-FLAG®M2-Peroxidase (HRP) (Sigma) antibody to detect TMK1-FLAG and with anti-PIN2 antibody to detect co-immunoprecipitated endogenous PIN2.

Tobacco leaves were infiltrated or co-infiltrated with overnight LB suspensions of *Agrobacterium tumefaciens* GV3101 carrying the desired expression plasmids (*35S::ABL3-HA*, *35S::ABL3-mCherry*, *35S::TMK1-HA*, *35S::TMK1-mCherry*). Including an overnight dark incubation, the infiltrated plants were grown for 36 hours, and leaves were subsequently harvested in liquid nitrogen. Frozen leaves were ground on ice in ice-cold extraction buffer (50 mM Tris-HCl, pH 7.6, 150 mM NaCl, 10 % glycerol, 5 mM DTT, 1 mM PMSF, 0.5 % NP-40, complete Roche protease inhibitors). The extracts were centrifuged in a tabletop centrifuge at top speed for 15 min and the supernatant was harvested, followed by a repetition of the same. The protein extracts were incubated with ChromoTek RFP-Trap Magnetic Agarose (rtma-20, Proteintech) for 1 hour at 4 °C (rotating), washed 5 times with the extraction buffer, and analyzed by SDS-PAGE. Blotting was with an Abcam anti-mCherry antibody (ab167453) and anti-HA-HRP (described above).





Active ROP assay on non-overexpressing plants

5-day-old seedling roots were harvested and incubated in ½ MS liquid medium with 100 nM IAA or mock treatment for 10 minutes and frozen in liquid nitrogen. Total protein was extracted in extraction buffer (25 mM HEPES pH 7.4, 100 mM KCl, 10 mM MgCl₂, 1 mM PMSF, 5 mM Na3VO4, 5 mM NaF, 1 mM TCEP, cOmplete rotease Inhibitor Cocktail, Roche) in 2 steps. For every 100 mg of ground tissue, 400 μl of extraction buffer was added, then incubated with another 400 μl of extraction buffer containing 5% Triton X-100 for one hour. Active ROP proteins were pulled down using His-MBP-CRIB (BL21 *E. coli* total cell extract) conjugated to HisPurTM Ni-NTA Magnetic Beads (Thermo Fisher) by incubation of 200 μl total protein extract with 25 μl (initial volume) of beads for 2 hours at 4°C. The beads were washed with Washing buffer (25 mM HEPES pH 7.4, 300 mM KCl, 10 mM MgCl₂, 12.5 mM imidazole) 3 times and boiled at 95°C with 30 μl SDS loading dye (BioRad). Protein samples were separated by 12% SDS-PAGE and analyzed by immune-blotting with an anti-ROP2 antibody (1:10,000, Abiocode). Input samples were blotted for total ROP2 content.

Recombinant protein expression and purification from *E. coli*

The 6xHis-PIN2 HL recombinant protein was expressed using the 6xHis-PIN2 HL vector⁸³ in *E. coli* BL21 (DE3) strain upon induction by 0.5 mM IPTG (isopropyl β -D-1-thiogalactopyranoside) at 16°C for 12 h. Cells were harvested by centrifugation at 4000 g for 15 min and washed with water. They were then lysed by sonication in lysis buffer (50 mM Tris-HCl pH7.5, 150 mM NaCl, 1 mM EDTA, 1 mM DTT, and 1% Triton X-100). The lysed solution was centrifuged at 12000 g for 15 min. The supernatant was then purified using Ni-NTA His affinity agarose (Thermo Scientific) according to the manufacturer's instructions. 6xHis-PIN2 HL protein was eluted from the beads in elution buffer (50 mM Tris-HCl pH7.4, 150 mM NaCl, and 250 mM imidazole). Eluted protein samples were checked by SDS-PAGE and Coomassie brilliant blue staining (Bio-SafeTM Coomassie Stain, Bio-Rad). The protein concentration was determined with the Bradford method (Quick StartTM Bradford Reagent, Bio-Rad).

TMK1-HA immunoprecipitation

To immunoprecipitate HA-tagged TMK1 protein, roots of 7-day-old UBQ10::TMK1-3xHA and $DEX::TMK1^{K616R}$ -HA (previously induced for 48 h with 30 μ M dexamethasone) seedlings were frozen and ground in liquid nitrogen, and subsequently homogenized in protein extraction buffer [PEB: 50 mM Tris-HCl pH7.5, 200 mM NaCl, 1% Triton X-100, 10 mM MgCl₂, 1 mM MnCl₂, Complete (Roche) protease cocktail and PhosSTOP phosphatase inhibitor cocktail (Roche)), followed by a 20 min centrifugation step at 14000 g, 4°C. In a fresh Eppendorf tube, 50 μ L anti-HA agarose beads were added (Anti-HA Affinity Matrix, SIGMA; pre-washed with 200 μ L PEB) to the supernatant. After 4 h of rotating at 4°C, the samples were spun down again at 2000 g, 4°C, and the supernatant was discarded. The agarose beads were washed twice with 200 μ L PEB, and finally re-suspended into 50 μ L PEB for further work.

In vitro kinase assay

The *in vitro* kinase assay with $[\gamma^{-32}P]$ -ATP was conducted as reported ⁸³ with minor modifications. Immunoprecipitated TMK1-HA and TMK1^{K616R}-HA (5 μ L) from 7-day-old Arabidopsis seedlings, together with the recombinant 6xHis-PIN2 HL (10 μ L) from *E. coli*, were added to the kinase reaction buffer (50 mM Tris-HCl pH 7.5, 10 mM MgCl₂, 5 mM NaCl, 2.5 mM cold ATP (adenosine 5'-triphosphate), and 1 mM DTT) in the presence of 5 μ Ci $[\gamma^{-32}P]$ -ATP (NEG502A001MC; Perkin-Elmer). Reactions were incubated at 25°C for 90 min and terminated by adding 10 μ L 5×SDS loading buffer. 20 μ L reaction samples were then separated with 10% SDS-PAGE gel, developed with a phosphor-plate overnight. Eventually, the phosphor plate was imaged with a Fujifilm FLA 3000 plus DAGE system.

Statistical analysis

Data processing and visualization was done in R version 4.0.4.

Accession Numbers

Gene sequence data from this article can be found in the Arabidopsis Genome Initiative databases under the following accession numbers: AT4G02980 (*ABP1*), AT1G66150 (*TMK1*), AT1G24650 (*TMK2*), AT2G01820 (*TMK3*), AT3G23750 (*TMK4*), AT5G57090 (*PIN2*), AT1G20090 (*ROP2*), AT4G35020 for (*ROP6*), AT4G30190 (*AHA2*), AT5G46330 (*FLS2*), AT1G72610 (*ABL1*), AT5G20630 (*ABL2*), AT4G14630 (*ABL3*).





Supplemental figures

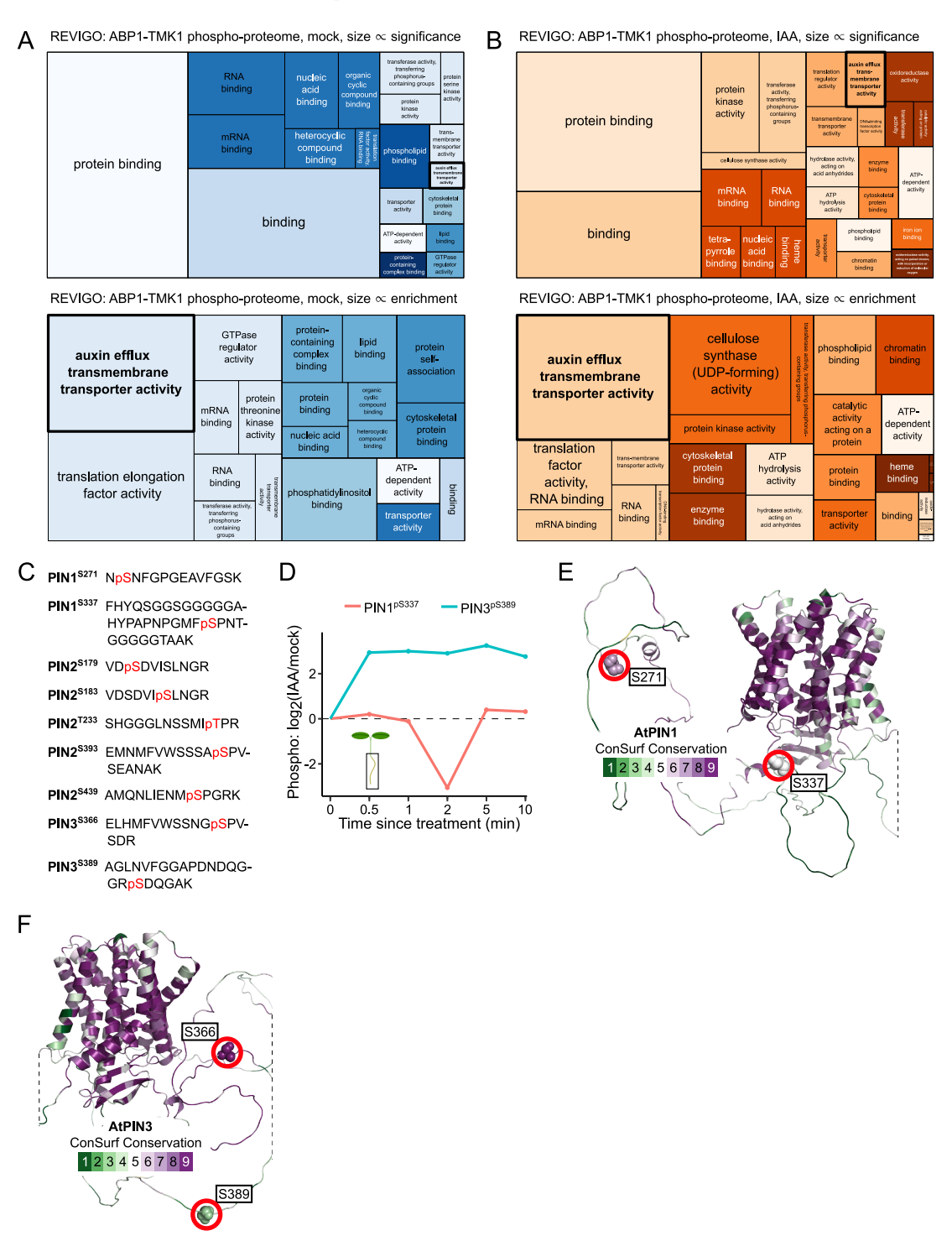


Figure S1. Identification of PINs as ABP1-TMK1 phospho-targets by GO analysis, related to Figure 1

(A) REVIGO treemap of GO terms enriched for the ABP1-TMK1 phospho-proteome under mock conditions. Box sizes scale with -log10(p value) (top) or fold enrichment (bottom).



⁽B) REVIGO treemap of GO terms enriched for the ABP1-TMK1 phospho-proteome under auxin treatment (100 nM IAA, 2 min) conditions. Box sizes scale with —log10(p value) (top) or fold enrichment (bottom).

⁽C) Overview of phospho-peptides pertaining to PIN phospho-sites from Figure 1A.

⁽D) Significant PIN1 and PIN3 phospho-site auxin profiles (FDR \leq 0.01, 100 nM IAA).

⁽E) Localization of ABP1-TMK1-dependent phospho-sites on a ConSurf conservation-colored AlphaFold2 structure of PIN1.

⁽F) Localization of ABP1-TMK1-dependent phospho-sites on a ConSurf conservation-colored AlphaFold2 structure of PIN3.





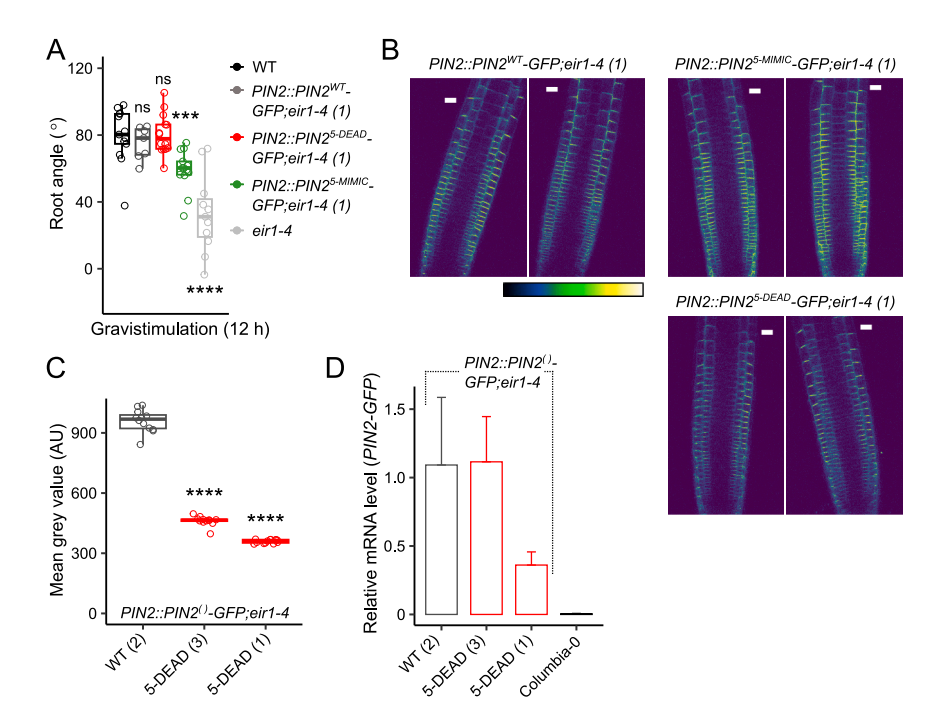


Figure S2. Supplementary data on PIN2-GFP phospho-lines, related to Figure 2

(A) Normalized root angles after 12-h gravistimulation of PIN2-GFP phospho-lines or WT (Col-0) on medium with sucrose (1%). Kruskal-Wallis analysis followed by Holm-corrected Wilcoxon rank sum tests relative to WT. *p < 0.05, **p < 0.01, ****p < 0.001, ****p < 0.0001.

(B) Representative median root sections showing PIN2-GFP phospho-line polarity. Scale bar, 20 µm.
(C) Quantification of GFP signal in two independent PIN2^{S-DEAD}-GFP phospho-lines compared with a PIN2^{WT}-GFP phospho-line. Kruskal-Wallis analysis followed by Holm-corrected Wilcoxon rank sum tests relative to the PIN2^{WT (2)}-GFP phospho-line. *p < 0.05, **p < 0.01, ****p < 0.001, ****p < 0.0001. a.u., arbitrary units. (D) qPCR quantification of PIN2-GFP mRNA in phospho-lines corresponding to (C). No PIN2-GFP was amplified in a WT Col-0 sample. The Kruskal-Wallis analysis result was significant ($\chi^2 = 9.359$, df = 3, p = 0.02488), but neither post hoc comparison with Holm-corrected Wilcoxon rank sum tests relative to PIN2^{WT (2)}-GFP was significant (all p > 0.05). Mean \pm SD.



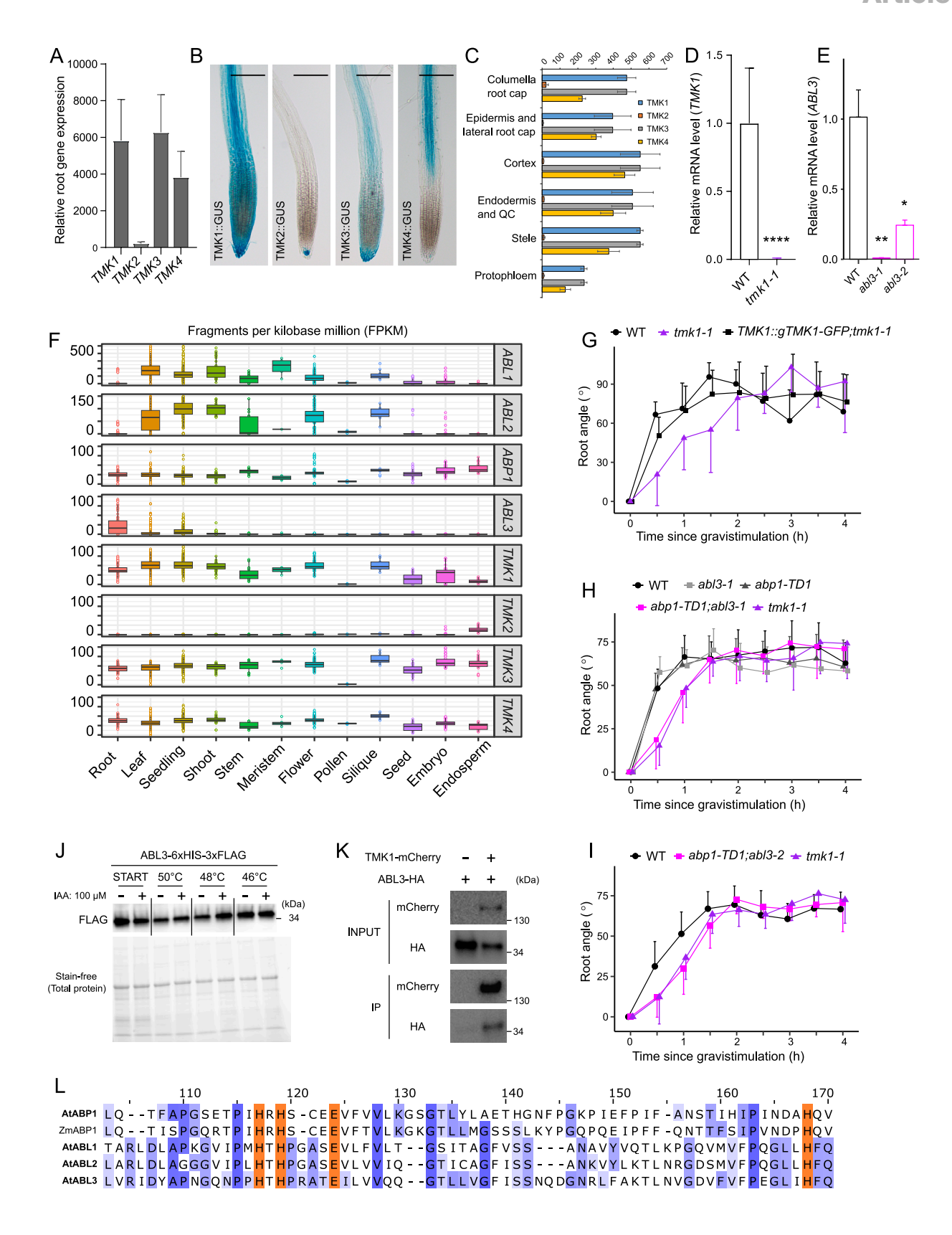






Figure S3. Expression of TMK genes and analysis of the tmk1-1 mutant, related to Figure 3

(A) Relative transcription levels of *TMK1*, *TMK2*, *TMK3*, and *TMK4* in *Arabidopsis* roots from 803 samples assayed with the Affymetrix *Arabidopsis* ATH1 Genome Array. Data were obtained using the Genevestigator databases (https://genevestigator.com). Mean + SD.

- (B) Root tip expression pattern of TMK1, TMK2, TMK3, and TMK4 promoters fused to the GUS transcriptional reporter. Scale bar, 100 µm.
- (C) Relative expression levels of *TMK1*, *TMK2*, *TMK3*, and *TMK4* in different root cell types obtained from high-resolution spatiotemporal microarray analysis of 5-to 6-day-old roots reported in Brady et al.⁸⁴ (ePlant http://bar.utoronto.ca/eplant).
- (D) qPCR quantification of *TMK1* mRNA in *tmk1-1*. Wilcoxon rank sum test (****p < 0.0001). Mean \pm SD.
- (E) qPCR quantification of ABL3 mRNA in T-DNA insertion lines abl3-1 and abl3-2. Kruskal-Wallis analysis followed by Holm-corrected Wilcoxon rank sum tests relative to WT. $^*p < 0.05$, $^*p < 0.01$. Mean \pm SD.
- (F) Comprehensive expression profiles of ABP1/ABL/TMK genes obtained using Arabidopsis RNA-seq libraries from Zhang et al. 75
- (G) Root gravitropism profiles on medium without sucrose. Mean \pm SD.
- (H) Mutant root gravitropism profiles on medium without sucrose. Mean \pm SD.
- (I) Mutant root gravitropism profiles on medium without sucrose. Mean \pm SD.
- (J) CETSA-based binding assay for protection from thermal denaturation on 35S::ABL3-6xHIS-3xFLAG seedlings in the presence of 100 μ M IAA.
- (K) CoIP from Arabidopsis root protoplasts of ABL3-HA with TMK1-mCherry but not with anti-mCherry beads alone.
- (L) Multiple sequence alignment of ABP1/ABL protein sequences surrounding the auxin pocket with metal-coordinating residues (orange). Purple coloring highlights conservation.



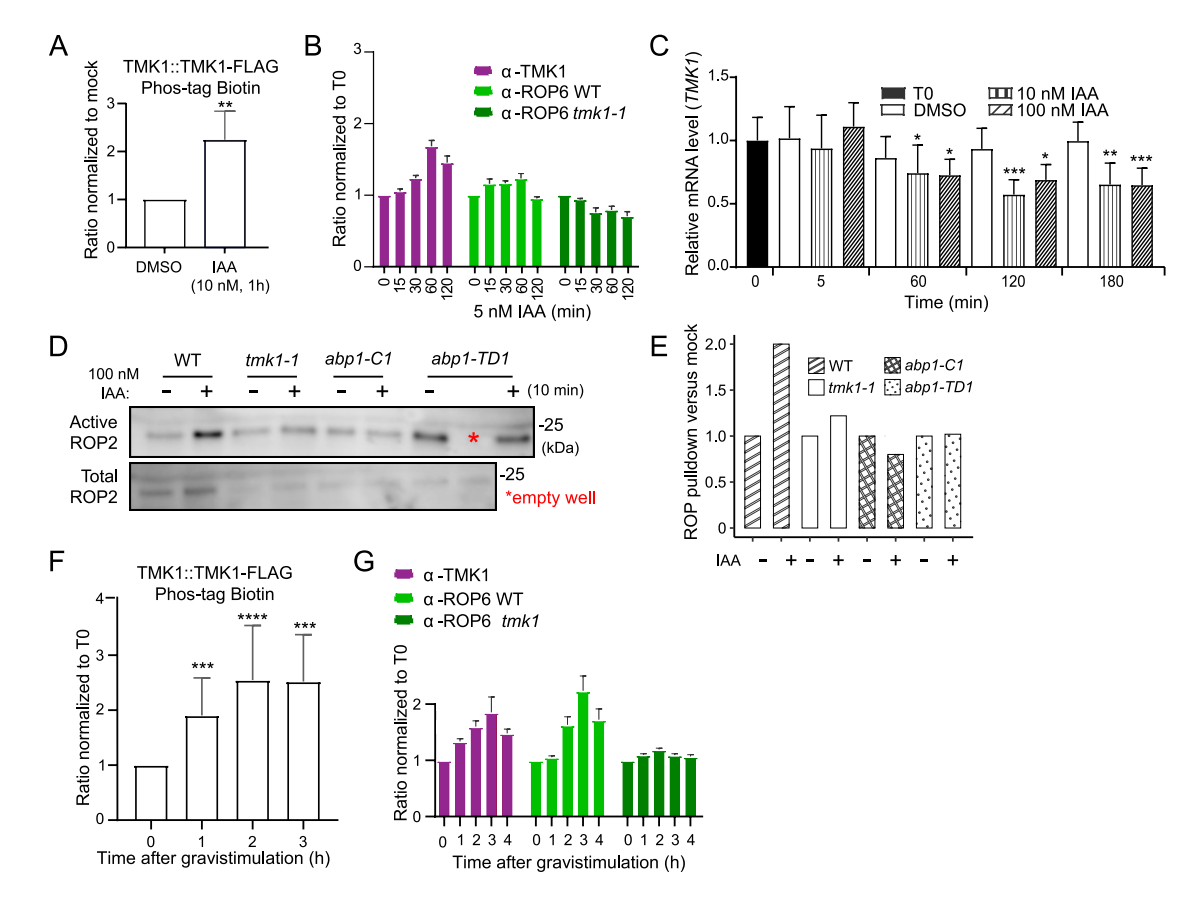


Figure S4. Supplementary data for ROP activation through TMK1, related to Figure 4

(A) Quantification of auxin effect on TMK1 phosphorylation in *TMK1::TMK1-FLAG;tmk1-1* roots assayed through TMK1-FLAG IP and Phos-tag Biotin Probe analysis. Phosphorylation levels detected with a Phos-tag Biotin Probe were normalized to the signal obtained from anti-FLAG detection and subsequently to the mock value. Mean + SD of 3 biological replicates. Wilcoxon rank sum test, **p < 0.01.

- (B) Quantification of auxin effect on ROP6 and TMK1 levels in the WT or *tmk1-1* root microsomal protein fractions. Band intensities were normalized to the loading control and subsequently to the respective first time point (T0). Mean + SD of 3 biological replicates.
- (C) qPCR of TMK1 expression after auxin treatment. The expression level at the start of the experiment (T0) was set to a relative value of 1. Mean \pm SD. Multiple comparison tests are relative to the first time point (T0). *p < 0.05, **p < 0.001, ****p < 0.001.
- (D) Auxin effect on ROP2 activation assayed by native ROP pull-down from roots of the indicated genotypes. Related to Figure 4C.
- (E) Quantification of the ROP pull-down assay depicted in (D) and Figure 4C. Active ROP2 levels were normalized to total ROP2 levels. For each genotype, normalized active ROP2 levels under mock conditions were set to a relative value of 1.
- (F) Quantification of gravistimulation effect on TMK1 phosphorylation in TMK1::TMK1-FLAG;tmk1-1 roots assayed through TMK1-FLAG IP and Phos-tag Biotin Probe analysis. Phosphorylation levels detected with a Phos-tag Biotin Probe were normalized to signal obtained from anti-FLAG detection and subsequently to the first time point (T0). Mean + SD of 3 biological replicates. Wilcoxon rank sum tests (****p < 0.0001).
- (G) Quantification of gravistimulation effect on ROP6 and TMK1 levels in the WT or tmk1-1 root microsomal protein fractions. Band intensities were normalized to the loading control and subsequently to the first time point, T0. Mean \pm SD of 3 biological replicates.

Cell Article



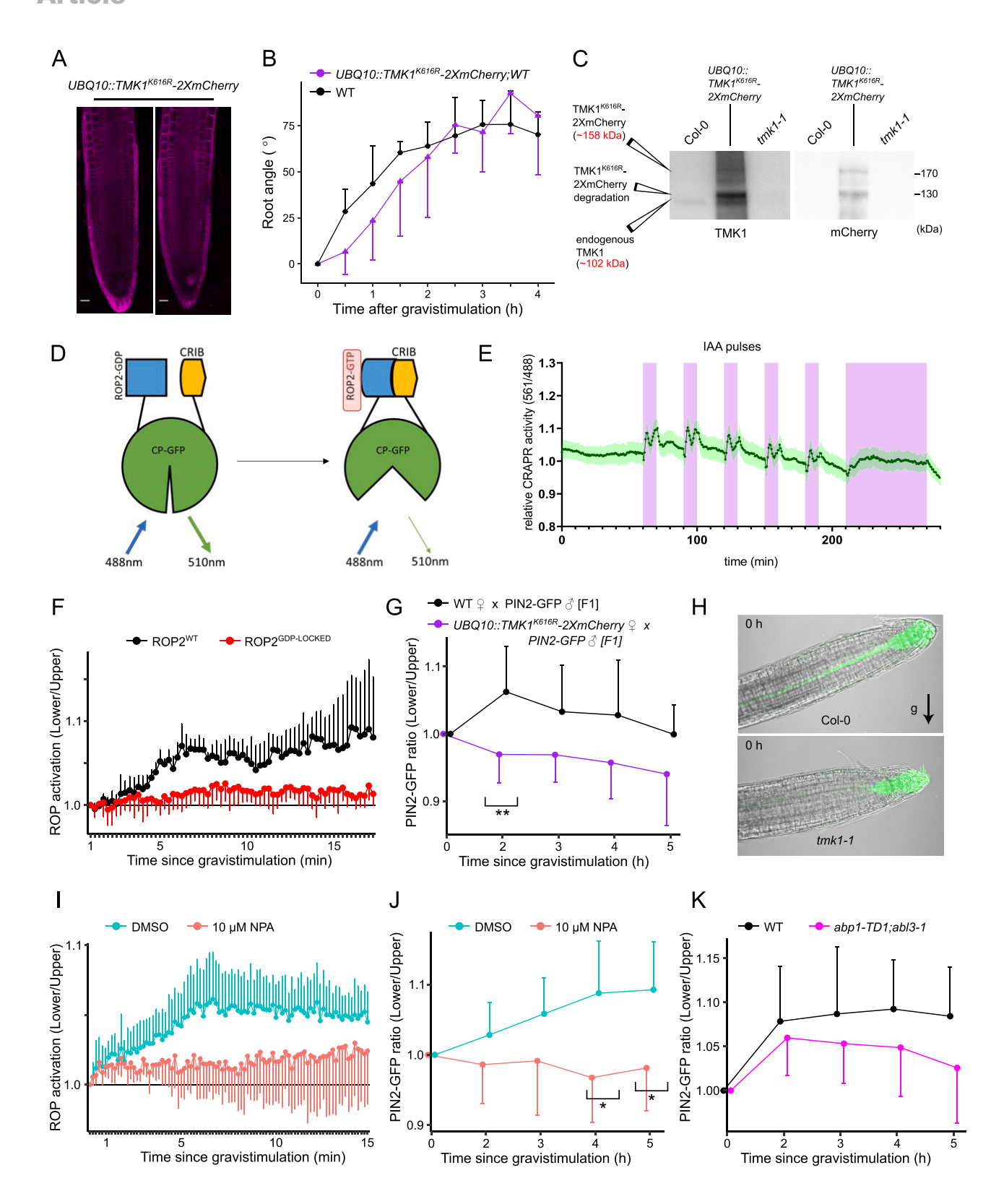


Figure S5. Requirement of TMK1 kinase activity for early root gravitropism, related to Figure 5
(A) Representative images of primary roots expressing the *UBQ10::TMK1*^{K616R}-*mCherry* construct. Scale bar, 20 μm.
(B) Root gravitropism profiles on medium without sucrose. Mean ± SD.





(C) Western blotting shows that native TMK1 protein expression is not silenced in *UBQ10::TMK1*^{K616R}-*mCherry* roots. Note that this experiment employed a different anti-TMK1 antibody (biosite/THP medical, ASJ-FADMZZ-100) than other experiments in the manuscript (affinity-purified antibody from Cao et al. ⁵⁷).

⁽D) Schematic showing the function of the CRAP sensor.

⁽E) CRAP sensor reports IAA pulses (10 nM IAA, highlighted in magenta) in a microfluidic root chip device.

 $⁽F) \ Dominant-negative \ mutation \ in \ the \ CRAP \ sensor \ abolishes \ rapid \ gravistimulation-induced \ establishment \ of \ CRAP \ asymmetry \ in \ WT \ roots. \ Mean \ \pm \ SD.$

⁽G) Dominant-negative effect of $UBQ10::TMK1^{K616R}$ -mCherry on gravistimulation-induced PIN2-GFP asymmetry. Mean \pm SD. Holm-corrected Wilcoxon rank sum tests were used to compare the normalized ratios between the two genotypes for each time point except T0. Only significant differences are reported. **p < 0.01.

⁽H) Representative confocal images of DR5rev::GFP;WT and DR5rev::GFP;tmk1-1 roots before gravistimulation.

⁽I) 10 μ M NPA treatment abolishes rapid gravistimulation-induced establishment of CRAP asymmetry in WT roots. Mean \pm SD.

⁽J) 10 μ M NPA treatment abolishes gravistimulation-induced PIN2-GFP asymmetry. Mean \pm SD. Holm-corrected Wilcoxon rank sum tests were used to compare the normalized ratios between the two treatments for each time point except T0. Only significant differences are reported. *p < 0.05.

⁽K) PIN2-GFP asymmetry defect in abp1-TD1; abl3-1 double mutant. Mean \pm SD. Holm-corrected Wilcoxon rank sum tests were used to compare the normalized ratios between the two genotypes for each time point except T0. Before Holm adjustment, only the difference for the 5-h time point was significant (p = 0.0212), but multiple hypothesis correction rendered it insignificant (p = 0.0848).



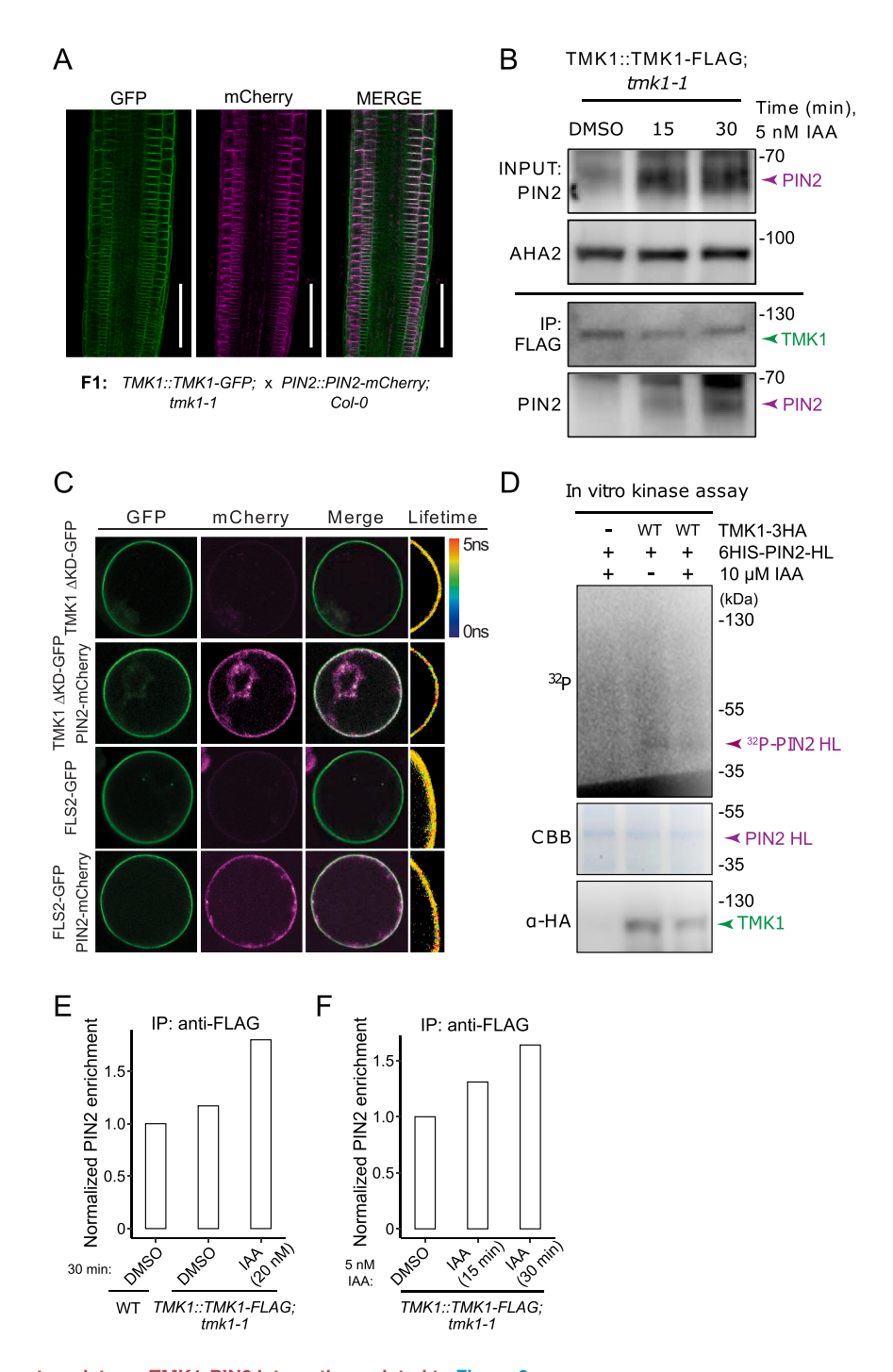


Figure S6. Supplementary data on TMK1-PIN2 interaction, related to Figure 6

(A) Co-localization of TMK1-GFP and PIN2-mCherry expressed from native promoters. Scale bar, 100 μm .

(B) CoIP assay showing the interaction of TMK1 with PIN2 upon low auxin treatment (5 nM IAA).

(C) FRET-FLIM analysis on transiently expressed 35S::TMK1^{ΔKD}-GFP, 35S::TMK1^{ΔKD}-GFP/35S::PIN2-mCherry, 35S::FLS2-GFP, and 35S::FLS2-GFP/35S:: PIN2-mCherry in root protoplasts. GFP fluorescence lifetime was calculated as described in the STAR Methods section. The heatmap depicts fluorescence lifetime values.

(D) In vitro kinase assay showing phosphorylation of the 6His-PIN2 HL substrate by TMK1-3xHA in the presence or absence of auxin. Top, ³²P-autoradiography; middle, CBB staining; bottom, immunoblot with an anti-HA antibody.





⁽E) Quantification of coIP experiment from Figure 6A. The enrichment of immunoprecipitated PIN2 was calculated by taking a ratio to AHA2(loading)-normalized input PIN2 levels.

⁽F) Quantification of coIP experiment from (B). The enrichment of immunoprecipitated PIN2 was calculated by taking a ratio to AHA2(loading)-normalized input PIN2 levels.